Strain partitioning in a large intracontinental strike-slip system accommodating backarc-convex orocline formation: The Circum-Moesian Fault System of the Carpatho-Balkanides

Nemanja Krstekanić, Liviu Matenco, Uroš Stojadinović, Ernst Willingshofer, Marinko Toljić, Daan Tamminga

10.1016/j.gloplacha.2021.103714

Global and Planetary Change 208 (2022) 103714

Contents lists available at ScienceDirect

Global and Planetary Change

journal homepage: www.elsevier.com/locate/gloplacha

Strain partitioning in a large intracontinental strike-slip system accommodating backarc-convex orocline formation: The Circum-Moesian Fault System of the Carpatho-Balkanides

Nemanja Krstekanić [a,b,*], Liviu Matenco [a], Uros Stojadinovic [b], Ernst Willingshofer [a], Marinko Toljić [b], Daan Tamminga [a]

[a] Utrecht University, Faculty of Geosciences, Utrecht, the Netherlands
[b] University of Belgrade, Faculty of Mining and Geology, Belgrade, Serbia

ARTICLE INFO

Editor: Zhengtang Guo

Keywords:
Oroclines
Strain partitioning
Strike-slip
Indentation
Carpatho-Balkanides
Circum-Moesian Fault System

ABSTRACT

The evolution of oroclines is often driven by the interplay of subduction and indentation associated with complex patterns of deformation transfer from shortening to strike-slip and extension. We study the kinematics and mechanics of indentation in an orocline with a backarc-convex geometry, the European Carpatho-Balkanides Mountains. Within this orocline, the kinematic evolution of the Serbian Carpathians segment is less understood. The results demonstrate that the overall deformation was accommodated by the Circum-Moesian Fault System surrounding the Moesian indenter, where strain was partitioned in a complex network of coeval strike-slip, thrust and normal faults. This system represents one of the largest European intracontinental strike-slip deformation zones, with a northward-increasing accumulated 140 km dextral offset along previously known and newly found faults. These strike-slip faults transfer a significant part of their offset eastwards to thrusting in the Balkanides and westwards to orogen-parallel extension and the formation of intramontane basins. The correlation with paleogeographic and geodynamic reconstructions demonstrates that the overall formation of the fault system is driven by subduction of the Carpathian embayment, resulting in laterally variable amounts of translation and rotation associated with indentation of the Moesian Platform. The onset of Carpathian slab retreat and backarc extension at 20 Ma has dramatically increased the rates of dextral deformation from ~3.5 mm/yr to ~2 cm/yr, facilitated by the pull exerted by the retreating slab. Our study demonstrates that indentation requires a strain partitioning analysis that is adapted to the specificity of deformation mechanics and is, therefore, able to quantify the observed kinematic patterns.

1. Introduction

The indentation of continental fragments is commonly used to explain orogenic shortening and crustal/lithospheric thickening accompanied by lateral extrusion, which is often associated with opposite polarity subduction systems (Davy and Cobbold, 1988; Doglioni et al., 2007; Faccenna et al., 2014; Johnson, 2002; Jolivet et al., 2018; Molnar and Tapponier, 1975; Regard et al., 2005). Indentation tectonics is observed in many orogenic systems (e.g., Argand, 1924; McKenzie, 1972; Ratschbacher et al., 1991a, 1991b). For instance, the indentation of the Indian indenter is accommodated by shortening and uplift of the Himalayas and Tibet, and lateral extrusion towards SE Asia (Chen et al., 2000; Molnar and Tapponier, 1975; Searle et al., 2011; Shen et al., 2001; Sternai et al., 2016; Tapponnier et al., 1986), shortening in front of the Arabian indenter is accompanied by Anatolian extrusion towards the Aegean (Kaymakci et al., 2010; Mantovani et al., 2006; Martinod et al., 2000; Regard et al., 2005), or the post-Oligocene shortening in the Eastern Alps is accompanied by extrusion towards the Pannonian-Carpathians region (Frisch et al., 1998; Neubauer et al., 2000; Ratschbacher et al., 1991b; Rosenberg et al., 2018; van Gelder et al., 2020; Wölfler et al., 2011). The lateral transfer of collisional shortening to other subduction systems is often facilitated by a complex strike-slip and transpressional/transtensional deformation associated with significant strain partitioning (e.g., Jolivet et al., 2018; van Hinsbergen et al., 2020; van Unen et al., 2019a). Similar to many other studies (e.g., Benesh et al., 2014; Cembrano et al., 2005; D'el-Rey Silva

* Corresponding author at: Utrecht University, Faculty of Geosciences, Utrecht, the Netherlands.
E-mail address: n.krstekanic@uu.nl (N. Krstekanić).

https://doi.org/10.1016/j.gloplacha.2021.103714
Received 23 June 2021; Received in revised form 16 November 2021; Accepted 21 November 2021
Available online 29 November 2021

et al., 2011; De Vicente et al., 2009; Glen, 2004; Krézsek et al., 2013), we use the term strain partitioning in its general meaning of a multi-scale distribution of the total strain in different types of coeval structures whose kinematics cannot be explained by a homogenous stress field. Such cases of strain partitioning and deformation transfer during indentation include the Dinarides orogen that transfers the deformation from the Alps to the Aegean subduction (van Unen et al., 2019a), the East Anatolian and the Dead Sea Faults that accommodate deformation along the lateral margin of the Arabian indenter (Lyberis et al., 1992; Perinçek and Çemen, 1990; Smit et al., 2010) or the Sagaing Fault of Indochina that connects India/Eurasia collision with the Sunda subduction system (Morley, 2002, 2013; Morley and Arboit, 2019; Vigny et al., 2003). Although kinematics along individual faults is well studied, the mechanisms of deformation transfer from shortening in front of an indenter to strike-slip along its lateral margins and the effects of indenter's geometry on strain partitioning are still not fully understood.

One remarkable example of deformation transfer from frontal shortening to lateral strike-slip along the margins of an indenter is the

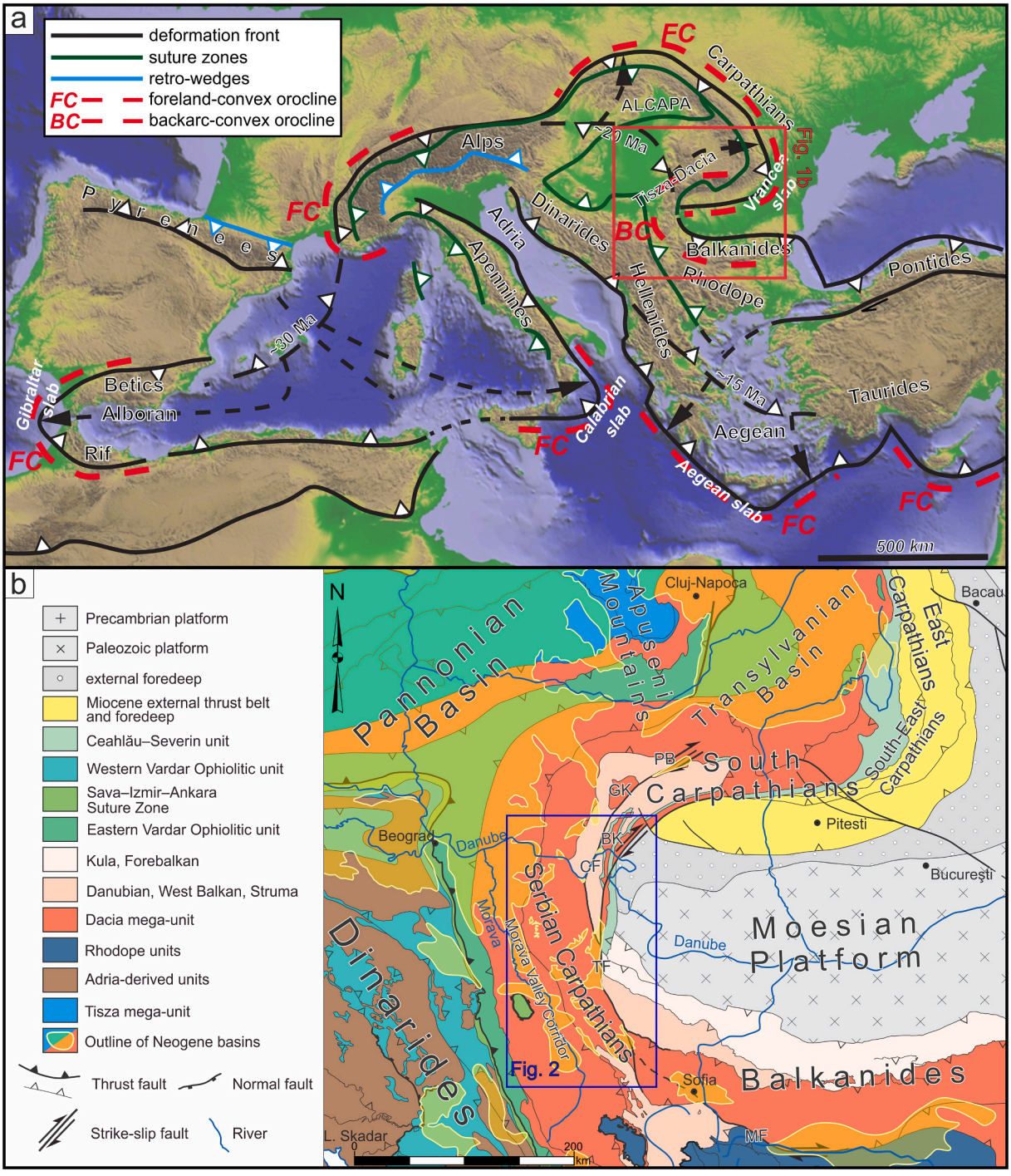

Fig. 1. a) Simplified European topographic map overlain by tectonic key elements (orogenic fronts, suture zones and retro-shears) of the Mediterranean Alpine-age orogens (modified from Krstekanić et al., 2020). The red rectangle shows the location of Fig. 1b. b) Regional tectonic map of the Carpatho-Balkanides orocline (modified after Schmid et al., 2020). The blue rectangle indicates the location of Fig. 2. BK - Bahna Klippe; CF - Cerna Fault; GK - Godeanu Klippe; MF - Maritsa Fault; PB - Petroşani Basin; TF - Timok Fault. (For interpretation of the references to colour in this figure legend, the reader is referred to the web version of this article.)

Carpatho-Balkanides orocline of south-eastern Europe. This double 180° curved orogenic system is comprised of a foreland-convex segment in the north and east, and a backarc-convex segment in the south and west (Fig. 1a). In our definition, a foreland-convex orocline has the convex side oriented towards the foreland (i.e., the vergence of the main orogenic structure is away from its core), while a backarc-convex orocline has the convex side oriented towards the backarc region (i.e., the orogenic thrusting is towards the oroclinal core, see also Krstekanić et al., 2020). The foreland- and backarc- convex oroclines are geometrically similar to a pair of salient – recess geometries (e.g., Marshak, 1988; Miser, 1932; Weil and Sussman, 2004). The later terms are used to describe the curvature of a single thrust front or a fold-and-thrust belt that is often related to thin-skinned thrusting and controlled by the footwall basin geometry and rheological variability (e.g., Livani et al., 2018; Marshak, 1988; Yonkee and Weil, 2010). In contrast, we use foreland- and backarc- convex oroclines to describe the geometry of larger scale curvatures that include rotations during orogenic build-up (i.e., oroclinal bending).

The overall formation of the Carpatho-Balkanides backarc-convex orocline was associated with the late Oligocene – middle Miocene formation of one of the largest strike-slip systems known in continental Europe, which accumulated more than 100 km of dextral offset along the curved Cerna and Timok Faults system (Fig. 1b, Berza and Drăgănescu, 1988; Kräutner and Krstić, 2002, 2003; Ratschbacher et al., 1993). The Serbian Carpathians were coevally affected by orogen-parallel and orogen-perpendicular extension that formed numerous Oligocene-Miocene intra-montane basins and the prolongation of the Pannonian Basin along the Morava Valley Corridor (Figs. 1b, 2; Erak et al., 2017; Krstekanić et al., 2020; Matenco and Radivojević, 2012). The connected and neighbouring structures of the western Balkanides recorded contraction during their thrusting over the Moesian Platform (Figs. 1b, 2; Schmid et al., 2020).

All these deformations associated with the ultimate formation of the Carpatho-Balkanides backarc-convex oroclinal bending created a large fault system where contrasting types of deformation affected the orogenic system and are connected around the southern, western and northern margins of the Moesian Platform (Fig. 1b). We herewith define this deformation associated with large-scale strain partitioning as the Circum-Moesian Fault System (CMFS), which is made up of a complex network of coeval strike-slip, thrust and normal faults. The mechanics and kinematics of this fault system and its strain partitioning along the Moesian margins are not understood. To advance this understanding, we have performed a field kinematic and structural study, focused on quantifying the CMFS deformation in the less understood area of the Serbian Carpathians, which links the deformation in the South Carpathians in the northeast to deformation in the Balkanides in the southeast. We correlate our results with previously published studies from the neighbouring East Carpathians, Rhodope, Dinarides, Pannonian Basin and Morava Valley Corridor (Fig. 1b, e.g., Brun and Sokoutis, 2007; Ellouz et al., 1994; Erak et al., 2017; Krstekanić et al., 2020; Matenco and Radivojević, 2012; Necea et al., 2021; Stojadinovic et al., 2013, 2017) to infer the relative importance of deformation in these regions on strain partitioning in our study area and to discuss potential mechanisms driving the formation of the backarc-convex Carpatho-Balkanides orocline. Because the formation of this backarc-convex orocline is rather unique during the Alpine evolution of the entire Mediterranean area (see Fig. 1), the results are shortly discussed in a larger regional and process-oriented context.

2. Tectonic evolution of the Carpatho-Balkanides during oroclinal bending and Moesian indentation

Previous studies have shown that most of the South and Serbian Carpathians and Balkanides mountains are made up of the large Europe-derived, Dacia continental mega-unit (Fig. 1b) that split-off during the Middle Jurassic opening of the Ceahlău–Severin branch of the Alpine Tethys Ocean, while to the west and south-west this mega-unit was separated from the Adria microcontinent by a northern branch of the Neotethys Ocean, which started to open during Middle Triassic times (Schmid et al., 2008, 2020; van Hinsbergen et al., 2020 and references therein). The Carpatho-Balkanides orogen (Fig. 1a) formed during the Cretaceous – Miocene closure of the Alpine Tethys Ocean (Csontos and Vörös, 2004; Horváth et al., 2015; Maţenco, 2017). The initial late Early Cretaceous partial closure of the Ceahlău–Severin branch in the South and Serbian Carpathians and Balkanides segments of the orogen created a thick-skinned nappe-stack and was facilitated by the collision with Moesian Platform, a promontory of the stable European continent, which acted as indenter during the collision (Fig. 1b, Csontos and Vörös, 2004; Săndulescu, 1988; Schmid et al., 2020). Shortening of the Dacia mega-unit created two main thick-skinned units, i.e., the Supragetic and Getic nappes of the South and Serbian Carpathians (see also Kräutner and Krstić, 2002). The nappe-stacking was followed by Late Cretaceous extension and calc-alkaline magmatism (in the Apuseni-Banat-Timok-Sredna Gora belt, see Gallhofer et al., 2015; von Quadt et al., 2005) and a latest Cretaceous overthrusting of the Dacia mega-unit over the Ceahlău–Severin nappe and Moesia that created a Danubian nappe-stack derived from the Moesian margin (Fig. 1b, Csontos and Vörös, 2004; Săndulescu, 1988; Seghedi et al., 2005). These Cretaceous events were followed by the continuation of oceanic subduction and Miocene slab retreat in the Western and Eastern Carpathians, which facilitated the creation of the southern backarc-convex orocline during 90 degrees of clockwise rotation and docking of the South Carpathians against the Moesian indenter (Fig. 1, Balla, 1984, 1986; Csontos et al., 1992; Krstekanić et al., 2020; Márton, 2000; Panaiotu and Panaiotu, 2010; Pătraşcu et al., 1994; Ratschbacher et al., 1993; van Hinsbergen et al., 2020). The oroclinal bending was associated with a Paleocene-Eocene orogen-parallel extension that exhumed the Danubian nappes of the South Carpathians (Fig. 1b; Fügenschuh and Schmid, 2005; Matenco and Schmid, 1999; Schmid et al., 1998) and the late Oligocene – middle Miocene creation of the curved Cerna and Timok Faults system (Fig. 1b).

2.1. The Cretaceous multi-phase nappe structure, extension and associated magmatism

The remnants of the Ceahlău–Severin Ocean are thought to outcrop in two regions within our studied area (Figs. 2 and 3, see also Schmid et al., 2020). In the north-eastern region situated in the vicinity of the Danube River, these remnants are composed of the uppermost Jurassic – Lower Cretaceous clastic to calcareous, locally ophiolite-bearing, turbiditic sequences (Bogdanović and Rakić, 1980; Kalenić et al., 1976; Melinte-Dobrinescu and Jipa, 2007; Săndulescu, 1984; Savu et al., 1985; Veselinović et al., 1975). In the southern part of the studied area west of the Kusa Vrana anticline (Fig. 2), Tithonian – Lower Cretaceous clastic to calcareous turbidites overlie the Danubian units and are thrusted by the Getic nappe of the Dacia-mega unit (Anđelković et al., 1977; Petrović et al., 1973; Vujisić et al., 1980).

The late Early Cretaceous (~100–110 Ma) thrusting of the Supragetic over the Getic units was top to ~E in the present-day geometry of the Serbian Carpathians (Figs. 2 and 3, Krstekanić et al., 2020, and references therein). The Supragetic basement is made up of Variscan mostly greenschist to sub-greenschist facies metamorphic rocks (e.g., Iancu et al., 2005b), overlain by passive margin continental late Carboniferous – Permian clastics and, locally, thin Triassic – Jurassic shallow-water limestone sequences (Kalenić et al., 1980; Petković, 1975a; Veselinović et al., 1970). The Getic unit is locally separated in Upper and Lower Getic sub-units along a large, but variable offset, thrust (Fig. 2; Krstekanić et al., 2020). Both sub-units have a similar greenschist to amphibolitic metamorphic basement, intruded by *syn*- to post-collisional Variscan granitoids (~325–290 Ma; Iancu et al., 2005a, 2005b; Jovanović et al., 2019; Kräutner and Krstić, 2002). The sedimentary cover is composed of Permian alluvial red clastics and transgressive Lower – Middle Triassic shallow-water sediments overlain by

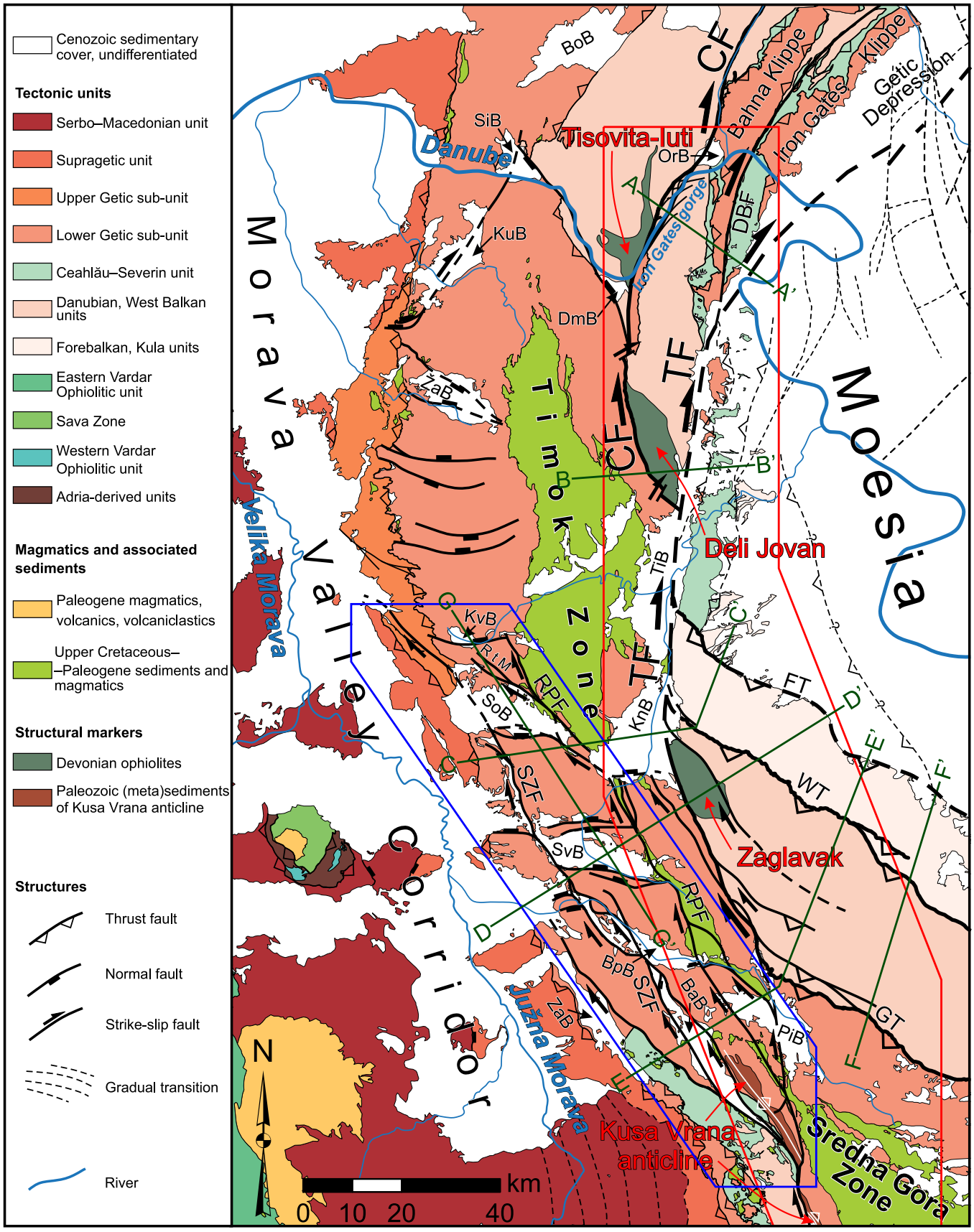

(caption on next page)

Fig. 2. Tectonic and structural map of the Serbian Carpathians and adjacent areas showing the regional fault kinematics of the Circum-Moesian Fault System (CMFS, compiled and modified after Basic geologic map of former Yugoslavia, scale 1:100.000, Maţenco, 2017, Krstekanić et al., 2020, following the terminology of Schmid et al., 2020 and the results of this study). Red polygon is the location of Fig. 4, blue polygon marks the location of Figs. 6 and 8. Dark green lines show positions of cross-sections in Fig. 3. BaB – Babušnica Basin; BoB – Bozovici Basin; BpB – Bela Palanka Basin; CF - Cerna Fault; DBF - Dževrin-Balta Fault; DmB – Donji Milanovac Basin; FT - Forebalkan Thrust; GT - Getic Thrust; KnB – Knjaževac Basin; KuB – Kučevo Basin; KvB – Krivi Vir Basin; OrB – Orşova Basin; PiB – Pirot Basin; RPF - Rtanj-Pirot Fault; RtM – Rtanj Mountains; SiB – Sichevița Basin; SoB – Sokobanja Basin; SvB – Svrljig Basin; SZF - Sokobanja-Zvonce Fault; TF - Timok Fault; TiB – Timok Basin; WT - West Balkan Thrust; ZaB – Zapljanje Basin; ŽaB – Žagubica Basin. (For interpretation of the references to colour in this figure legend, the reader is referred to the web version of this article.)

Middle Jurassic transgressive clastics and carbonates, Upper Jurassic – Lower Cretaceous deep water to reef limestones and dolomites (Fig. 3, e.g., Antonijević et al., 1970; Grădinaru et al., 2016; Krstić et al., 1976; Petković, 1975b; Veselinović et al., 1970; Vujisić et al., 1980). The total thickness of the Getic sedimentary cover reaches ~2 km.

The Carpatho-Balkanides recorded a Late Cretaceous phase of calc-alkaline magmatism, genetically interpreted to be related to the roll-back of the Neotethys subducting slab, or alternatively by the variability of the subduction in the Ceahlau-Severin Ocean, which created the so-called Apuseni–Banat–Timok–Sredna Gora (ABTS) magmatic belt (Andrić et al., 2018; Balla, 1984, 1988; Berza et al., 1998; Gallhofer et al., 2015; Kolb et al., 2013.; Neubauer, 2015; Toljić et al., 2018; von Quadt et al., 2005). In the study area, this magmatism is observed in the Timok and Sredna Gora zones (Figs. 2 and 3), where the Upper Cretaceous – Paleogene intrusives, volcanics and volcaniclastics are associated with coeval normal faulting (Banješević, 2006; Kalenić et al., 1976; Knaak et al., 2016; Kräutner and Krstić, 2003; Petković, 1975b; Veselinović et al., 1975). To the west, this extension is thought to have exhumed the amphibolite facies metamorphics of the Serbo-Macedonian unit (peak metamorphism of Variscan age, ~480–330 Ma; Antić et al., 2016a) from below the Supragetic unit in the footwall of detachments (Fig. 2; Antić et al., 2016a, 2016b; Erak et al., 2017). The Serbo-Macedonian unit is also part of the Dacia mega-unit and, together with the obducted Eastern Vardar Ophiolitic unit, forms the upper plate in respect to the Neotethys subduction along the Sava suture zone of the Dinarides (Figs. 1, 2; Pamić, 2002; Stojadinovic et al., 2017; Schmid et al., 2008; Ustaszewski et al., 2010).

Renewed shortening took place during the latest Cretaceous (~75–67 Ma), postdating the extension and magmatism in the ABTS belt (Iancu et al., 2005a; Neubauer and Bojar, 2013; Schmid et al., 2008), which created the Supragetic-Getic-Danubian nappe stack (Figs. 2 and 3, Ciulavu et al., 2008; Csontos and Vörös, 2004; Berza et al., 1983; Maţenco, 2017; Săndulescu, 1984). The basement of Danubian units has recorded several deformation events and poly-phase metamorphism and is built of high-grade Neoproterozoic Pan-African and low-grade Caledonian to Variscan metamorphic rocks with a weak Alpine metamorphic overprint (Dallmeyer et al., 1998; Iancu et al., 2005a, 2005b; Kräutner and Krstić, 2002; Ratschbacher et al., 1993; Seghedi et al., 2005). This metamorphic basement includes also the pre-Alpine granitic intrusions and Devonian Tisovita-Iuti – Deli Jovan – Zaglavak ophiolitic complex (Iancu et al., 2005b; Kalenić et al., 1976; Kräutner and Krstić, 2002; Krstić et al., 1976; Plissart et al., 2017; Seghedi et al., 2005; Zakariadze et al., 2012), whose location is important for restoring the below described post-Eocene oroclinal deformation (Figs. 2 and 3). The Danubian metamorphic basement is overlain by continental to shallow-water lacustrine Permian clastics, lower Triassic clastics and Middle to Upper Triassic carbonates, a Lower to Middle Jurassic clastic succession, Middle Jurassic to late Early Cretaceous carbonates and locally Late Cretaceous fine-grained sediments (Fig. 3, Anđelković et al., 1977; Bogdanović and Rakić, 1980; Iancu et al., 2005a; Kalenić et al., 1976; Krstić et al., 1976; Veselinović et al., 1975).

2.2. The Eocene–Miocene oroclinal bending

Following the Cretaceous orogeny, subduction of the Carpathian embayment lithosphere and continental collision continued in the Western and Eastern Carpathians during Paleogene-Miocene times. The nature of the subducted slab is still debated and could have had oceanic or highly extended continental character (e.g., Bokelmann and Rodler, 2014; Necea et al., 2021). The N-, N*E*- and E-ward Miocene roll-back and closure of the Carpathian embayment have created ultimately the two oroclines observed in the double Carpatho-Balkanides loop (Fig. 1a; Ustaszewski et al., 2008). While the South Carpathians segment underwent a coeval gradual clockwise rotation of up to 90° (e.g., Balla, 1984, 1986, 1987; de Leeuw et al., 2013; Dupont-Nivet et al., 2005; Pătraşcu et al., 1990, 1992, 1993; Panaiotu and Panaiotu, 2010), this rotation decreases to 25°-30° in the Serbian Carpathians segment and becomes negligible in the Balkanides (Lesić et al., 2019; van Hinsbergen et al., 2008).

The Paleocene – Eocene orogen-parallel extension reactivated the inherited basal thrust of the Getic unit in the South Carpathians and exhumed the Danubian nappe-stack along an extensional detachment, forming the Danubian window (Figs. 1b, 2; Fügenschuh and Schmid, 2005; Matenco and Schmid, 1999; Moser et al., 2005; Schmid et al., 1998). During the late extensional exhumation of the Danubian nappes, the main Eocene nappe stacking of the Balkanides took place, which truncated or partly reactivated the late Early Cretaceous thrusts and was followed likely by renewed thrusting in the West Balkans unit (Burchfiel and Nakov, 2015; Schmid et al., 2020; Vangelov et al., 2013). The orogen-parallel extension was followed by the formation of late Oligocene – early middle Miocene high offset curved strike-slip dextral Cerna and Timok Faults (Figs. 1b, 2 and 3; Berza and Drăgănescu, 1988; Kräutner and Krstić, 2002; Ratschbacher et al., 1993). The 35 km late Oligocene offset of the Cerna Fault and 65 km late Oligocene – early Miocene offset along the Timok Fault are documented by displaced Devonian ophiolites in the Danubian/West Balkan units basement (Tisovita-Iuti, Deli Jovan and Zaglavak, see Fig. 2) or by displaced South Carpathians nappe stack and intramontane basins (Berza and Drăgănescu, 1988; Kräutner and Krstić, 2002; Ratschbacher et al., 1993). The Timok Fault is thought to have transferred its offset to thrusting southwards in the Balkanides (e.g., Schmid et al., 2020, and references therein) and to transtension and extension in the frontal part of the South Carpathians (e.g., Rabăgia and Maţenco, 1999). Further away from the Moesian Platform, in the hinge of the backarc-convex orocline (i.e., the internal Serbian Carpathians), the strike-slip deformation was more distributed, previous studies being unable so far to identify regional-scale structures that may have accommodated significant strike-slip offsets (Mladenović et al., 2019; Krstekanić et al., 2020).

Dextral strike-slip displacement of the Cerna and Timok Faults was largely coeval with the Oligocene-Miocene orogen-perpendicular extension in the Pannonian Basin and its southern Morava Valley Corridor prolongation (Figs. 1b, 2 and 3), thought to have been driven by the coupled effect of the roll-back of Carpathian and Dinaridic slabs (Andrić et al., 2018; Balázs et al., 2016; Erak et al., 2017; Horváth et al., 2006; Matenco and Radivojević, 2012; Stojadinovic et al., 2013, 2017; Toljić et al., 2013). The *E*-W oriented extension in the Morava Valley Corridor started during the Oligocene (~29–27 Ma) and lasted until the middle Miocene (Erak et al., 2017; Matenco and Radivojević, 2012; Sant et al., 2018), affecting the internal segments (i.e., the hinge of the orocline) of the Serbian Carpathians (Krstekanić et al., 2020). Several lacustrine intramontane basins overlie the Cretaceous orogenic fold-and-thrust structure of the Serbian and South Carpathians (Figs. 2 and 3, Table 1). Among these, the oldest sediments are middle to upper Eocene lacustrine turbidites observed at the base of the Babušnica Basin

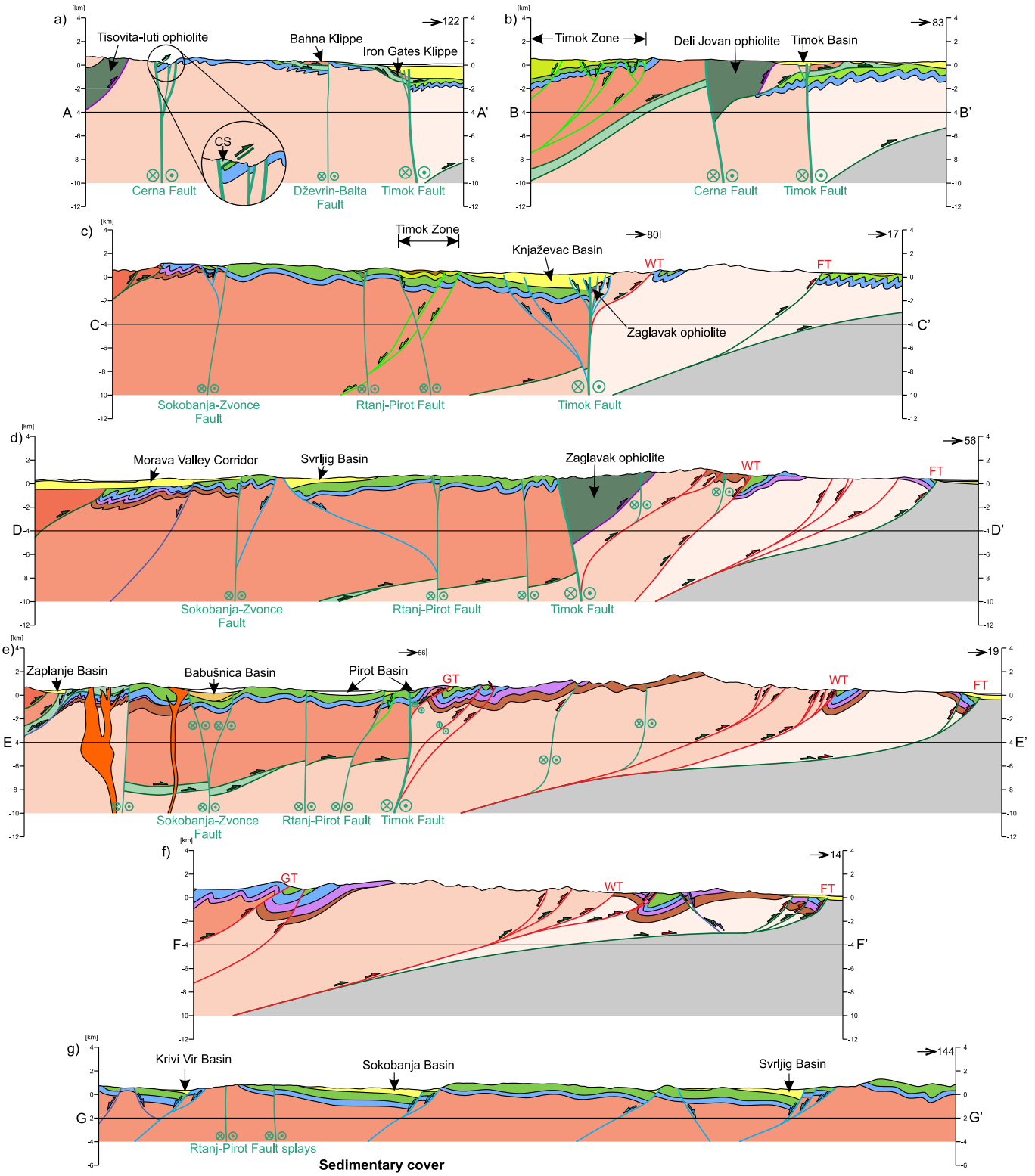

(caption on next page)

Fig. 3. Geologic cross-sections in the studied area. Surface to depth projection is based on the field kinematic data from this study and the Basic geologic map of former Yugoslavia, scale 1:100.000. The locations of the cross-sections are displayed in Fig. 2. The strike of each cross-section is indicated in the upper right corner of the section. No vertical exaggeration has been applied. FT - Forebalkan Thrust; GT - Getic Thrust; WT - West Balkan Thrust.

(Fig. 3e, Table 1; de Bruijn et al., 2018; Marković et al., 2017). Most of the other basins are filled with lower middle Miocene – Pliocene sediments, such as the Sokobanja, Žagubica and Svrljig Basins (Figs. 2, 3d, g, Table 1; Kalenić et al., 1980; Lazarević and Milivojević, 2010; Marković, 2003; Obradović and Vasić, 2007; Sant et al., 2018). The sedimentation in the Bela Palanka and Pirot basins is thought to have started only during Pliocene times (Table 1; Anđelković et al., 1977; Vujisić et al., 1980). Other basins are observed along the Cerna and Timok Faults, some connected with the coeval marine sedimentation overlying the Moesian Platform (Figs. 2, 3a-c). The middle Miocene Donji Milanovac and Orşova Basins opened along the Cerna Fault (Fig. 2, Table 1; Bogdanović and Rakić, 1980; Kräutner and Krstić, 2003), while the lower-middle Miocene sediments of the Timok and Knjaževac Basins (Krstić et al., 1976; Rundić et al., 2019; Veselinović et al., 1975) are truncated by and overlie the Timok Fault (Figs. 2, 3b, c). Previous studies have shown that some of the E-W trending basins (e.g., Žagubica, Krivi Vir, Sokobanja and Svrljig, Figs. 2 and 3g) were formed during a middle Miocene period of orogen-parallel extension, controlling their lacustrine deposition (Fig. 2; Krstekanić et al., 2020).

3. Methodology

3.1. The structural mapping approach

We have performed a field structural and kinematic analysis in the Serbian Carpathians and their transition to the Balkanides (Fig. 2). First, we identified the major faults or fault zones by using the existing 1:100.000 scale geologic maps (Basic geologic map of former Yugoslavia). These maps were also used for identifying other major regional structures (such as km-scale folds or uplifted and exhumed basement), correlations with neighbouring areas and for defining the timing of post-Cretaceous tectonic events by combining observations of stratigraphic offsets along faults and sealing post-kinematic deposits (see also Dimitrijević, 1997; Kräutner and Krstić, 2003; Schmid et al., 2008, 2020; Krstekanić et al., 2020 and references therein). The studied major structures include the curved dextral strike-slip Cerna and Timok Faults, two sub-parallel narrow (i.e., up to a few hundreds of meters wide) NNW-SSE oriented corridors of Paleogene to Miocene sediments and fault zones (the Sokobanja-Zvonce and Rtanj-Pirot Faults zones) and several E-W oriented normal faults bounding Miocene intramontane basins (Fig. 2). During fieldwork, we focussed on mapping the kinematics of large-offset faults and fault zones within post-Cretaceous sediments that are pre- to *syn*-kinematic to the observed faulting. Subsequently, we documented kinematics and the faulting superposition (by observing cross-cutting relationships, tilting, rotations and truncation) along the strike of these structures in the ophiolites, pre-Alpine granitoids and basement and the Mesozoic cover of the Getic and Danubian units (Fig. 2). We also investigated the middle Miocene intramontane basins, where we focused our mapping on the kinematics of the basin-controlling E-W oriented faults and their interaction with the connecting NNW-SSE oriented fault zones (Fig. 2). Furthermore, we mapped and analysed the kinematics of reactivated nappe contacts in the western Balkanides segment of the orocline (east and in the vicinity of the Timok Fault in Fig. 2).

All observed deformation has a brittle character. Field measurements include orientations of faults and fault zones, foliations within fault gouge and cataclasite, faulting-related cleavage and observations of tilting and rotations. Slickenside kinematic indicators (including calcite slickenfibres, grooves and other brittle indicators), Riedel shears and brittle shear bands in fault gouge and foliated cataclasite were used to

Table 1
Summarized ages of the intramontane basins in the South and Serbian Carpathians in Fig. 2. Ages are based on the correlations of geologic maps of former Yugoslavia and Romania, publications cited in the table and basins age synthesis in Krstekanić et al. (2020).

Basin	Sedimentary infill age	References
Babušnica	Initial infill: middle – upper Eocene (38–34 Ma) Middle stage: Oligocene (33–30 Ma) Final infill: Pliocene (~5 Ma)	de Bruijn et al. (2018); Marković et al. (2017); Vujisić et al. (1980)
Bozovici	Initial infill: lower Miocene? (~17–15 Ma) Main infill: lower middle Miocene (15–13 Ma)	Codrea (2001); Hír et al. (2016)
Bela Palanka	Early Pliocene (~5 Ma)	Vujisić et al. (1980)
Donji Milanovac	Lower middle Miocene	Bogdanović and Rakić (1980)
Knjaževac	Initial infill: lower Miocene (~17 Ma) Main infill (marine ingression): lower middle Miocene (15–13 Ma) Final infill: upper middle Miocene	Djurović and Živković (2013); Krstić et al. (1976); Rundić et al. (2019); Veselinović et al. (1975)
Kučevo	Initial infill: lower middle Miocene (15–13 Ma) Final infill: upper middle Miocene	Kalenić et al. (1980); Lazarević and Milivojević (2010)
Krivi Vir	Initial infill: late Oligocene (~24.5–23 Ma) Main and final infill: lower to upper Miocene?	Mai (1995); Veselinović et al. (1970); Žujović (1886)
Orşova	lower middle Miocene to upper middle Miocene	Geological map of Romania
Pirot	Early Pliocene (~5 Ma)	Anđelković et al. (1977)
Sicheviţa	Middle Miocene	Geological map of Romania
Sokobanja	Initial and main infill: lower middle Miocene (15–13 Ma) Final infill: upper Miocene? – Pliocene?	Krstić et al. (2012); Sant et al. (2018); Veselinović et al. (1970)
Svrljig	Initial and main infill: lower middle Miocene (15–13 Ma) Final infill: upper Miocene? – Pliocene?	Krstić et al. (1976); Krstić et al. (2012); Sant et al. (2018)
Timok	Initial infill: lower Miocene (~17 Ma) Main infill (marine ingression): lower middle Miocene (15–13 Ma) Final infill: upper middle Miocene	Djurović and Živković (2013); Krstić et al. (1976); Rundić et al. (2019); Veselinović et al. (1975)
Zaplanje	Initial and main infill: lower middle Miocene (15–13 Ma) Final infill: upper Miocene? – Pliocene?	Obradović and Vasić (2007); Sant et al. (2018); Vujisić et al. (1980)
Žagubica	Initial and main infill: lower middle Miocene (15–13 Ma) Final infill: upper Miocene? – Pliocene?	Antonijević et al. (1970); Lazarević and Milivojević (2010); Sant et al. (2018)

derive the sense of shear along faults and fault zones by considering confidence criteria and quality ranks (e.g., Angelier, 1994; Doblas, 1998; Sperner and Zweigel, 2010). The fault-slip data was separated by superposition, timing criteria and consistency of slip direction and sense of slip. Data collected in outcrops (Supplementary Appendix A, B) located in proximity and along the same map-scale structure are analysed together. We grouped the analysed data into structures (circled numbers and points in Figs. 4, 6 and 8) that combine multiple observation points.

3.2. Deformation analysis

We focussed only on the post-Cretaceous and pre- late Miocene deformation related to the Cerna and Timok Faults system and their associated structures. The older pre-Cenozoic structures are discriminated by mapping in the major post-Cretaceous fault zones, observed superposition criteria and their comparison with the previously studied Cretaceous tectonic events, such as orogen-perpendicular shortening(s) that created the Carpatho-Balkanides nappe-stack or Late Cretaceous backarc extension (e.g., Schmid et al., 2008; Gallhofer et al., 2015; Mladenović et al., 2019; Krstekanić et al., 2020). The Oligocene – middle Miocene orogen-perpendicular extension is observed in the Morava Valley Corridor in the convex side of the orocline to decrease eastwards (Erak et al., 2017; Stojadinovic et al., 2013, 2017; Toljić et al., 2013), which is coeval with the activity of Cerna and Timok Faults (Mladenović et al., 2019; Krstekanić et al., 2020. This observation enabled a separation of kinematics of these different coeval expressions of strain partitioning during the oroclinal formation (see also Krstekanić et al., 2020). It is important to note that in most situations of cross-cutting, structures showing different kinematics (e.g., strike-slip and normal faults) or orientations (e.g., two sets of dextral strike-slip faults) mutually truncate each other in outcrops. In such cases, we associate these structures to the same tectonic event.

The post-Cretaceous kinematics observed in multiple outcrops along strike of the major faults is assigned to its specific expression at map scale, which enabled an analysis of strain partitioning observed along major faults or fault zones. The lateral correlation between outcrops is based on the character of deformation in similar lithologies (e.g., fault gouges versus individual fault planes or brittle shear bands) as well as on the compatibility of deformation and offsets observed in the field with the one at the map scale. We present the mapped fault-slip data as being the result of a single large tectonic event because the observed cross-cutting relationships of reported structures with significantly different kinematics (normal, strike-slip and reverse faults) do not allow their separation to different events. These relationships demonstrate that structures of different kinematics formed coevally in the same area, which is a typical indication for strain partitioning.

The type of strain partitioning often observed in our dataset is related to local vertical axis rotations of earlier segments of faults in the same fault zone, restraining and releasing bends, horse-tail geometries, step-overs, thrusting associated with tear-faulting, or drag folding. We provide solutions for the type of observed strain partitioning based on kinematic effects, such as folds or strata rotations observed in outcrops by connecting field data and carefully following the same structure along its strike. Further information on this strain-based approach is available in published kinematic studies (e.g., Krstekanić et al., 2020; van Gelder et al., 2015; van Unen et al., 2019a, 2019b).

The observed strain partitioning is not suitable for deriving paleostress directions by kinematic data stress inversion. Paleostress inversion methods require that fault-slip measurements are taken along faults that do not have large offsets (i.e., kilometres to tens of kilometres) that are comparable with the fault size (e.g., Twiss and Unruh, 1998), which contrasts with the measured kinematics along faults that have offsets reaching tens of kilometres. Kinematic measurements taken within wide, large offset fault zones do not satisfy the Wallace-Bott criteria (Yamaji, 2003, and references therein) and are often associated with strain partitioning during deformation. Furthermore, one of the assumptions of the paleostress inversion methods is that fault kinematic data is derived from independently slipping faults and that there is no fault interaction (Angelier, 1979, 1989), which contrasts with the observed fault system. In addition, lithological contrasts between rocks with contrasting strength, such as limestones and volcaniclastics are often activated by large-offset faults. All these paleostress methodology limitations are otherwise well-known (e.g., Célérier et al., 2012; De Vicente et al., 2009; Hippolyte et al., 2012; Jones and Tanner, 1995; Lacombe, 2012; Orife and Lisle, 2003; Sperner and Zweigel, 2010).

4. Kinematic observations

Our dataset is presented in relationship with the major (i.e. large offset) structures, which are the Cerna and Timok Faults (Figs. 4, 5), the NNW-SSE oriented Sokobanja-Zvonce and Rtanj-Pirot Faults (Figs. 6, 7a-g) and the *E*-W oriented normal faults controlling the formation of Miocene basins (Figs. 7g, h and 8). The kinematics of regional faults was used to construct seven regional cross-sections (Fig. 3), which are both perpendicular and parallel to the main orogenic structures. The structure at depth is constructed only from surface kinematic projections by following the definition of the main tectonic units and the observed lateral variability of stratigraphy. Therefore, the degree of uncertainty of these cross-sections increases with depth.

4.1. Connecting the Cerna and Timok strike-slip with the Balkanides thrusting

The curved Cerna and Timok Faults system offsets the Cretaceous nappe-stack, the late Cretaceous basin(s) and the Eocene extensional Danubian window (Figs. 2, 4). The strike of these faults changes from NE-SW in the north, N-S in the centre, to NW-SE in the south. All observed deformation related to these faults is dominantly associated with (sub-)vertical strike-slip faults (Fig. 4). In the main fault zones, we commonly observed numerous closely-spaced (i.e., at tens of centimetres distance) sub-vertical faults with fault gouges and similar kinematics (e.g., Figs. 5a, d), decametre-scale, corrugated and striated fault surfaces (e.g., Fig. 5b), or several metres thick fault gouge zones that often display foliation (Figs. 5c, f).

Deformation along the Cerna and Timok Faults is often partitioned along multiple (sub-)parallel strands (e.g., structures S1, S5 and S13 in Fig. 4) that accommodate variable offsets. High-angle to vertical dextral strike-slip faults that are parallel to the map-view orientation of the Cerna or Timok Faults are observed in all locations (colour 1 in Fig. 4). Numerous secondary structures oriented obliquely to the strike of the Cerna or Timok Faults are also observed (Fig. 4), which demonstrate the presence of associated structures with different kinematics and/or local strain partitioning by different styles of branching or splaying, local rotations and up to kilometre-scale negative or positive flower structures (e.g., S1 and S13 in Fig. 4).

The segment of the Cerna Fault running through the Iron Gates gorge of the Danube River and its flanks (Figs. 2, 4) offsets the Danubian basement to the NW from its Mesozoic sedimentary cover to the SE and has at least two major strands (S1, Fig. 4). The main strand is outcropping along the NW bank of the Danube, exposing a high-density dextral strike-slip zone (Fig. 5a) or decametre-scale fault surfaces visible over the gorge walls (Fig. 5b). Furthermore, this strand is associated with up to several meters thick, weakly foliated fault gouge often observed in granites (the Variscan Ogradena granite, Fig. 5c). In the same gorge area to the southeast, the SE Cerna Fault strand (S1, Fig. 4) shows a more distributed deformation without distinct high-strain fault gouge formation. Outcropping between these two strands, a narrow sliver of highly deformed uppermost Jurassic – Lower Cretaceous sediments of the Ceahlău–Severin unit is tectonically overlying the uppermost Danubian sedimentary cover (see zoom-in of Fig. 3a; see also Kräutner and Krstić, 2003). The overall map and cross-section geometry shows a

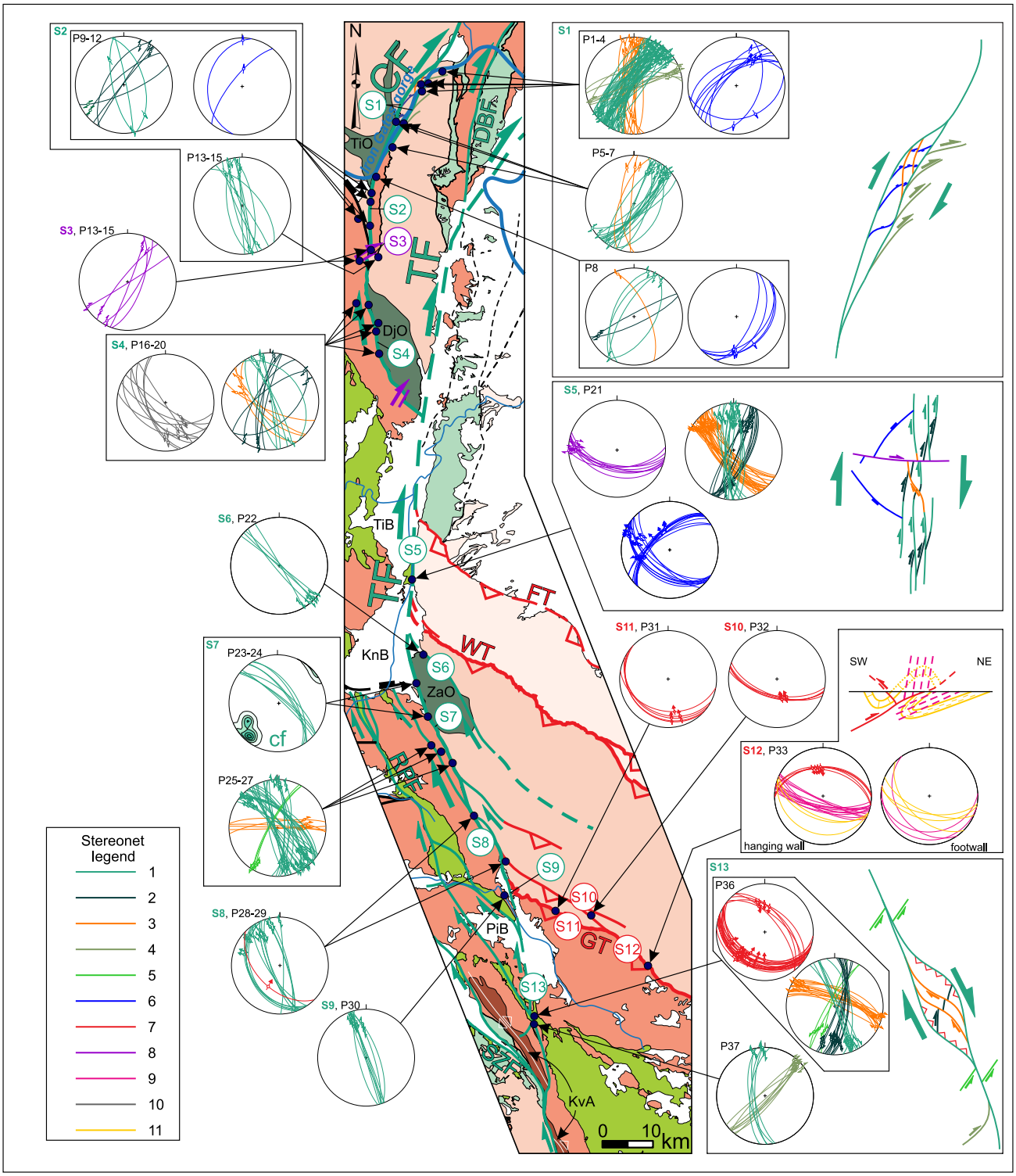

Fig. 4. Structural map of the Cerna and Timok Faults and neighbouring Balkanides thrusting areas with lower hemisphere stereographic projections of measured faults and foliations within fault gouge. The location of the map is displayed in Fig. 2. Faults covered by Neogene sediments or faults with unclear prolongation are dashed. Numbered structures in stereonets correspond to map-scale structures with the same number. Each structure may combine multiple observation points. S - structure; P - observation point; fault planes without a sense of shear are measured foliations within fault gouge; cf - density plot of the poles of foliation in fault gouge. Faults measured in outcrops are located within or correlated with faults at map-scale with the same kinematics. Their genetic interpretation follows the stereonet legend: 1 - faults parallel with the main map-scale dextral strike-slip fault, 2 - clockwise rotated dextral strike-slip faults within the main fault zone, 3 - faults connecting main fault strands, generally corresponding to the orientation of P- shears, 4 - dextral strike-slip faults splaying from the main fault zone, generally corresponding to the orientation of R-Riedel shears, 5 - conjugated sinistral strike-slip fault, 6 - normal fault with an oblique-slip component, 7 - thrusts and reverse faults with an oblique-slip component, 8 - late-stage NE-SW to E-W oriented dextral faults offsetting the main fault zones, 9 - cleavage, 10 - unclear structures, 11 - bedding. CF - Cerna Fault; DBF - Dževrin-Balta Fault; DjO - Deli Jovan ophiolite; FT - Forebalkan Thrust; GT - Getic Thrust; KnB - Knjaževac Basin; KvA - Kusa Vrana anticline; PiB - Pirot Basin; RPF - Rtanj-Pirot Fault; SZF - Sokobanja-Zvonce Fault; TF - Timok Fault; TiB - Timok Basin; TiO - Tisovita-Iuti ophiolite; WT - West Balkan Thrust; ZaO - Zaglavak ophiolite.

Fig. 5. Interpreted field photos of structures (and their stereographic projections) associated with the Cerna and Timok fault zones. Locations of photos are displayed in Fig. 4. The legend of fault colours is the same as in Fig. 4. a) Cerna Fault deformation zone along the flanks of the Iron Gates gorge in the NW fault strand at studied point P1. The fault zone affected Lower Cretaceous limestones by the formation of a pervasive high-angle to vertical foliation in fault gouge that displays often brittle senses of shear, plotted as fault planes with a sense of shear in the stereonet. b) Decametre scale fault plane with large scale striations and corrugations affecting Upper Jurassic limestones in the Cerna Fault zone along the flanks of the Iron Gates gorge in the NW at studied point P1. For the scale, note the two standing men in the black rectangle. c) Metres-thick fault gouge and foliation and zoomed detail in the Variscan Ogradena granite in the Cerna Fault zone along the NW flanks of the Iron Gates gorge at studied point P5. The position of the zoom-in photograph is indicated by the black rectangle. d) High-density fault system in Tithonian limestones along the Timok Fault zone at the eastern margin of the Timok and Knjaževac Basins at studied point P21. Deformation is characterized by decametre-scale N-S oriented faults (green) parallel to the Timok Fault, associated P-shears (orange) and transtensional normal faults (blue). e) Oblique normal faults in Tithonian limestones within the Timok Fault deformation zone along the eastern margin of the Timok and Knjaževac Basins at studied point P21. f) Fault gouge with sub-vertical foliation in the Devonian Zaglavak ophiolite (sheared and serpentinised gabbro) in the Timok Fault deformation zone at studied point P23. g) Oblique thrust in Tithonian limestones at studied point P29. h) Transfer of strike-slip deformation into thrusting in Jurassic limestones of the West Balkan unit at studied point P32. i) Overturned fold limb associated with low-angle pervasive axial plane cleavage in Lower Cretaceous marls in the footwall of the Getic Thrust at studied point P33. j) Sub-vertical and pervasive axial plane cleavage in Upper Jurassic limestones in hanging-wall of the Getic Thrust at studied point P33. k) Entrance to the Jerma gorge at studied point P36. Lower Cretaceous limestones building the flanks of the gorge are affected by strike-slip and thrust faulting in a large positive flower structure along the southern prolongation of the Timok Fault. l) WNW-ESE oriented dextral splay connecting two strands of the Timok Fault in the positive flower structure of the Jerma gorge at studied point P36. (For interpretation of the references to colour in this figure legend, the reader is referred to the web version of this article.)

dextral negative flower structure. Between the two main strands deformation is accommodated by connecting oblique normal faults or connecting P-shears (S1 in Fig. 4), while R-Riedel shears show splaying towards the NE (S1 in Fig. 4). Southwards, outcrop-scale faults follow the change in orientation of the Cerna Fault, which becomes more N-S oriented (S2, Fig. 4). Within the main fault zone, Cerna-parallel faults truncate earlier dextral faults rotated clockwise and are associated with few normal faults (S2, Fig. 4). Furthermore, the main N-S oriented Cerna

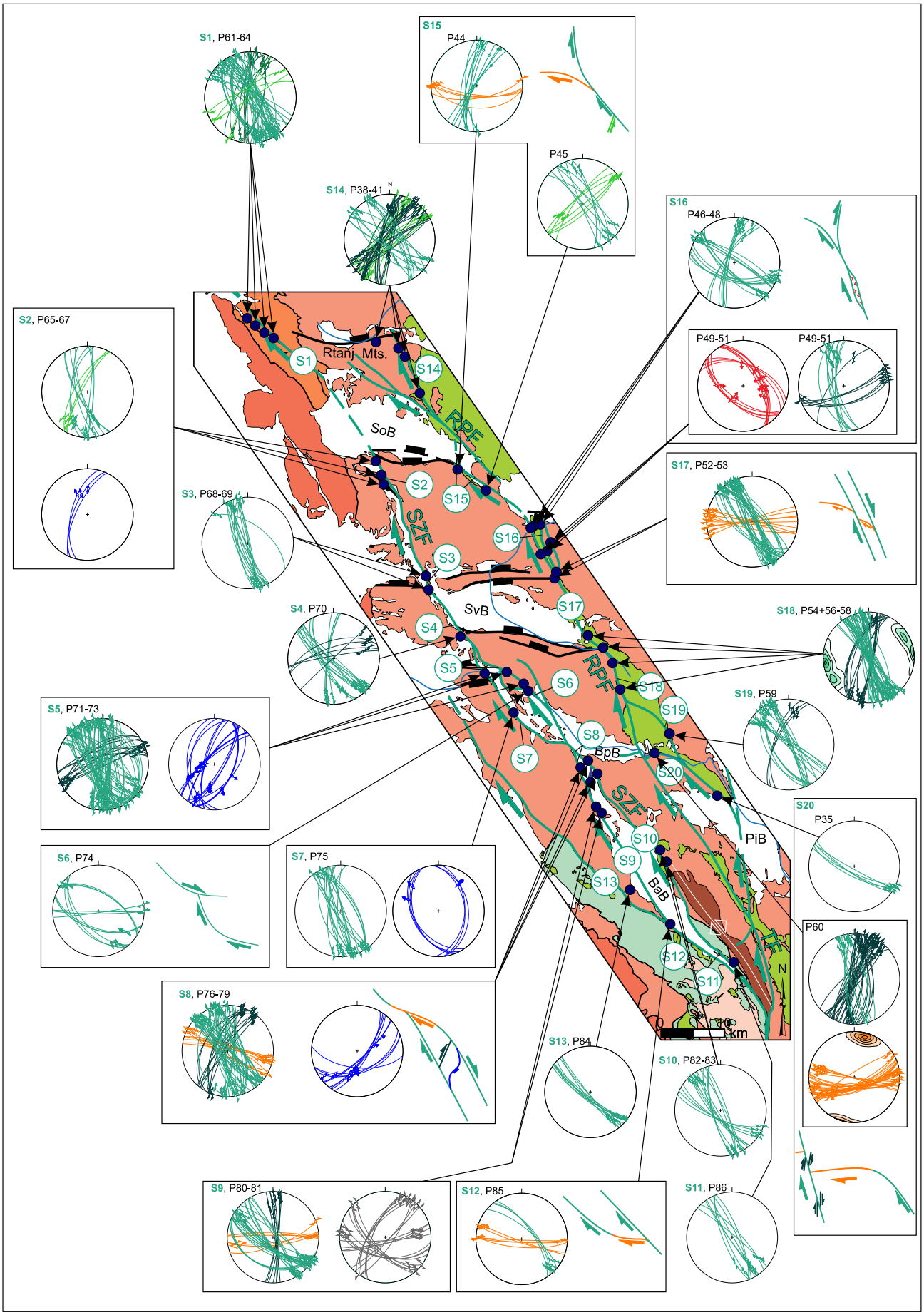

(caption on next page)

Fig. 6. Structural map and lower hemisphere stereographic projections of measured faults and foliations within fault gouge associated with the Sokobanja-Zvonce and Rtanj-Pirot strike-slip faults. The location of the map is displayed in Fig. 2. Faults covered by Neogene sediments or faults with unclear prolongation are dashed. Numbered structures in stereonets correspond to map-scale structures with the same number. Each structure may combine multiple observation points. S - structure; P - observation point. Fault planes without a sense of shear are measured foliations within fault gouge. Faults measured in outcrops are located within or correlated with faults at map-scale with the same kinematics. Stereonet legend is the same as in Fig. 4. BaB - Babušnica Basin; BpB - Bela Palanka Basin; PiB - Pirot Basin; RPF - Rtanj-Pirot Fault; SoB - Sokobanja Basin; SvB - Svrljig Basin; SZF - Sokobanja-Zvonce Fault; TF - Timok Fault.

Fault segment is offset by few hundred meters along a later NE-SW oriented dextral fault (S3, Fig. 4). Further south, the Cerna Fault changes its orientation to NW-SE and separates by dextral strike-slip the basement of the Getic unit to the west from the Danubian basement to the east. Along this segment, besides the Cerna-parallel, rotated faults or P-shears, all with a dextral sense of shear, a kinematically unclear type of likely sinistral normal faults have been observed outside and at farther distances from the main Cerna Fault zone (S4, Fig. 4).

Unlike the Cerna Fault, the Timok Fault is generally buried in its northern and central segments by the middle Miocene sediments of the Getic Depression and Timok and Knjaževac Basins. This is where the 65 km offset along this fault has been constrained by the distance between the truncated Deli Jovan and Zaglavak ophiolites (Fig. 4, see also Kräutner and Krstić, 2002). In this area, the Timok Fault crops out in one outlier at the transition between the Timok and Knjaževac Basins (S5, Fig. 4), where the N-S oriented Timok Fault separates the Forebalkan cover (Tithonian limestones) to the east from the Timok zone of the Getic unit (Turonian clastics) to the west. These Tithonian limestones are intensely deformed (Fig. 5d) by sub-vertical N-S oriented dextral strike-slip faults grouped in at least 3 closely spaced main strands that display decametre-scale fault surfaces. These strands are connected by splays and often truncate earlier, clockwise rotated, dextral faults, while the main fault zone is offset by late-stage E-W oriented dextral faults (S5, Fig. 4). The same area shows oblique, top to W or NW normal faults that are both truncated and truncate dextral faults (S5 in Fig. 4, see also Fig. 5d, e). The character of deformation remains similar south of the Knjaževac Basin until the Pirot Basin, but all structures are rotated to become parallel with the NNW-SSE Timok Fault main orientation. In this area, dextral strike-slip separates the Getic unit (Lower Cretaceous limestones) to the west from the West Balkan unit (the Zaglavak ophiolite, basement and Permian cover) to the east (Fig. 4). The deformation is distributed to discrete striated fault surfaces and rare foliated fault gouges (e.g., Fig. 5f). Most dextral faults and fault gauge foliations have the NNW-SSE Timok Fault orientation (S7–9, S13, Fig. 4), associated with obliquely oriented, clockwise rotated dextral faults, splays or conjugated sinistral faults (S7 and S13, Fig. 4). Further south, deformation associated with the Timok Fault is partitioned in two areas, associated with different sets of structures.

The first area is located immediately north of the Pirot Basin (Fig. 4), where structures document a gradual transfer from the top- N to NNW Srednogorie/Getic thrust (S10-12) to multiple splays changing gradually their kinematics westwards to reverse faults with a dextral component, which are ultimately connected to the NNW-SSE oriented Timok Fault (S8–9). For instance, this transfer can be observed by NW-SE dextral transpressive faults (Fig. 5g) that gradually change their orientation and get connected with top-NNW thrust faults in Jurassic limestones of the West Balkan unit to the SW (Fig. 5h), or by a pervasive cleavage associated with the same thrusting. The dip of this cleavage (high- versus low-angle) reflects a different degree of drag-folding in the footwall (Fig. 5i) versus the hanging-wall (Fig. 5j), as a function of different lithologies (shales versus limestones, respectively), associated locally with oblique S- to SSE-ward backthrusting (structure S12 in Fig. 4). Overall, the system of faults observed in this area documents a transfer of the top- N to NNW thrusting observed at the Getic/West Balkan contact (i.e., the Getic Thrust, Figs. 2-4) to the NNW-SSE oriented dextral offset along the Timok Fault.

South of the Pirot Basin, Timok-type deformation is observed in the Jerma river gorge in Tithonian to Lower Cretaceous limestones (S13, Fig. 4). Here, two main NNW-SSE oriented strands of the Timok Fault (Fig. 5k) are connected and change their orientation to NW-SE and kinematics to dextral transpressive to define a positive flower structure. The flower structure is associated with thrusts (Fig. 5k), connecting splays (Fig. 5l), conjugated sinistral faults and truncated, clockwise rotated, earlier dextral faults (S13, Fig. 4). In this area, the Timok Fault offsets the Kusa Vrana anticline axis by ~8 km (Fig. 4). This implies that only a small part of the 65 km Timok Fault offset measured north of the Pirot Basin can still be recognized southwards.

4.2. *Strike-slip deformation along the Rtanj-Pirot and Sokobanja-Zvonce Faults*

West and southwest of the Timok Fault, large, kilometres-sized offsets along dextral strike-slip faults are for the first time observed in our study along a larger array of ~NNW-SSE oriented structures. Among these structures, two have larger offsets and are herewith named the Rtanj-Pirot Fault and the Sokobanja-Zvonce Fault (RPF and SZF in Figs. 2, 6). Within these fault zones, deformation is transferred or partitioned along multiple strands and splays. Similar to the Cerna and Timok Faults, the character and type of deformation along these faults changes along their strike, often as a function of lithology, from tens of metres thick foliated fault gouges, pervasive (sub-) vertical faulting with similar kinematics to individual fault surfaces with striations (Fig. 7).

The most frequent structures are NNW-SSE oriented dextral faults, parallel to the map-scale orientation of the RPF and SZF (Fig. 6). These faults often truncate Upper Cretaceous or Paleogene strata (Fig. 7a, b) or tilt them to (sub-)vertical position (Fig. 7c). These dextral faults often display flower structure geometry (Fig. 7b). Similar to the Cerna and Timok Faults, these structures are associated with conjugated sinistral faults, earlier formed and clockwise-rotated dextral faults during the same dextral deformation, splays and dextral faults connecting different strands, as well as oblique thrusts and normal faults (Fig. 6). Earlier formed dextral faults are locally folded by dragging during the formation of splays (e.g., S6, Figs. 6 and 7d). The Rtanj-Pirot Fault is generally transpressive (e.g., the positive flower structure of Fig. 7b), while the Sokobanja-Zvonce Fault is generally transtensive, documented by oblique dextral-normal faults (S2, S5, S7, S8, Figs. 6 and 7e). The SZF bounds and controls the deposition in NNW-SSE oriented corridors filled with middle Miocene sediments (S2–7, Fig. 6), while truncating the Eocene deposits in the similarly oriented Babušnica Basin (S8–12 in Figs. 6 and 7e). Rtanj-Pirot and Sokobanja-Zvonce Faults are both connected with the Timok Fault to the SSE (Fig. 6).

Two strands of the Rtanj-Pirot Fault splay off of the Timok Fault in the SSE, while to the NNW they show secondary splays that are cross-cut by the western strand. The example of structure S20 (Fig. 6) shows that the eastern NNW-SSE oriented strand changes its orientation by splaying into an E-W oriented fault zone associated with ~15 m thick foliated fault gouge (Fig. 7f). This E-W splay is truncated or terminated by the other NNW-SSE oriented strand located to the west. Similar truncated or terminated splays can be observed also to the NNW (e.g., S17 in Fig. 6). The Rtanj-Pirot Fault terminates to the NNE by splaying and the formation of a horse-tail structure in the area of the Rtanj Mountains (S14 - S16, Fig. 6).

The Sokobanja-Zvonce Fault shows a similar interaction by the formation of two main strands that are connected to the Timok Fault in the SSE. These strands show locally truncated splays (e.g., S12 in Fig. 6), which get connected or split again to the NNW (S8 in Fig. 6). Besides

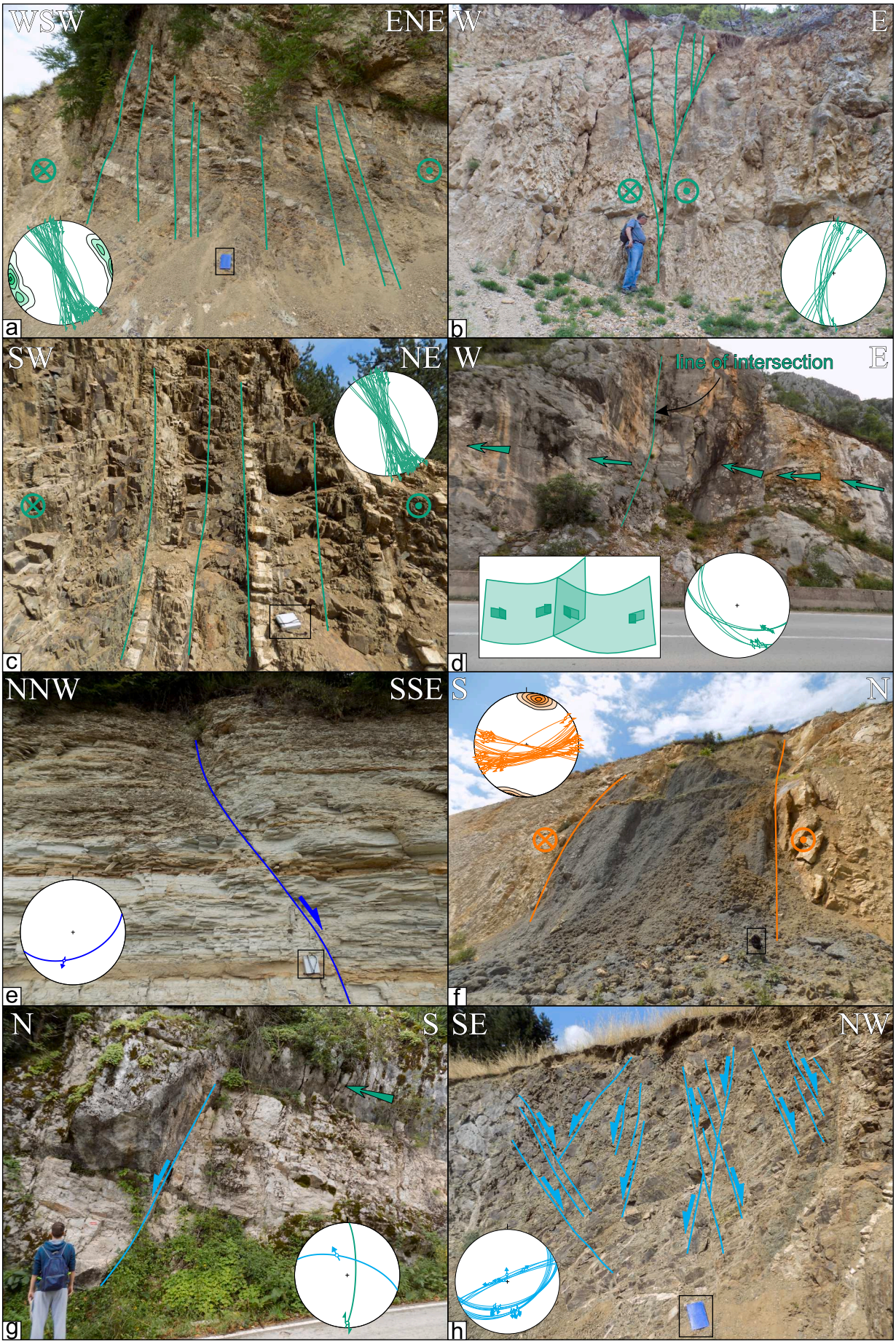

(caption on next page)

Fig. 7. Interpreted field photos of structures (and their stereographic projections) associated with the strike-slip and normal faulting. Locations of photos are displayed in Figs. 6 and 8. The legend of colours in stereonets is the same as in Fig. 4. a) Sub-vertical pervasive dextral faulting affecting Paleogene clastics along the Rtanj-Pirot Fault at studied point P54. Note the blue notebook in the black rectangle for scale. b) Positive flower structure in Upper Cretaceous volcaniclastics along the Rtanj-Pirot Fault at studied point P44. The entire outcrop is affected by pervasive sub-vertical faulting. c) Tilted sub-vertical bedding in Upper Cretaceous volcaniclastics with bedding-parallel dextral shearing along the Rtanj-Pirot Fault at studied point P56. d) Decametre-scale curved dextral faults in Lower Cretaceous limestones in the Sokobanja-Zvonce Fault zone at studied point P74. The observed curvature of one fault is achieved by dragging along the adjacent sub-parallel fault with the same or similar kinematics. e) Normal fault with oblique-slip component truncating upper Eocene-Oligocene sediments of the Babušnica Basin along the Sokobanja-Zvonce Fault at studied point P79. f) Faulted Lower Cretaceous limestones illustrating deformation associated with the Rtanj-Pirot Fault at studied point P60. The outcrop exposes ~15 m thick dextral fault gouge, which is a splay within the Rtanj-Pirot Fault zone (see structure S20, Fig. 6). Note the black backpack (in the black rectangle) for scale. g) Dextral strike-slip fault intersecting with a top-N normal fault in Lower Cretaceous limestones along the Sokobanja-Zvonce Fault at studied point P66. h) Low-offset conjugated normal faults in Upper Cretaceous volcaniclastics along the Rtanj-Pirot Fault at studied point P56. (For interpretation of the references to colour in this figure legend, the reader is referred to the web version of this article.)

dragging effects (e.g., S6, Figs. 6, 7d), often oblique-slip dextral normal faulting can be observed in the field to be associated with regional faults (e.g., S2, S5, S7, S8, Figs. 6, 7e). To the NNW, the Sokobanja-Zvonce Fault can be interpreted to flank both or one of the margins of the Miocene strike-slip corridors, while our interpretation assumes a continuation in the same direction from beneath the middle Miocene cover of the Sokobanja Basin (S1 in Fig. 6)

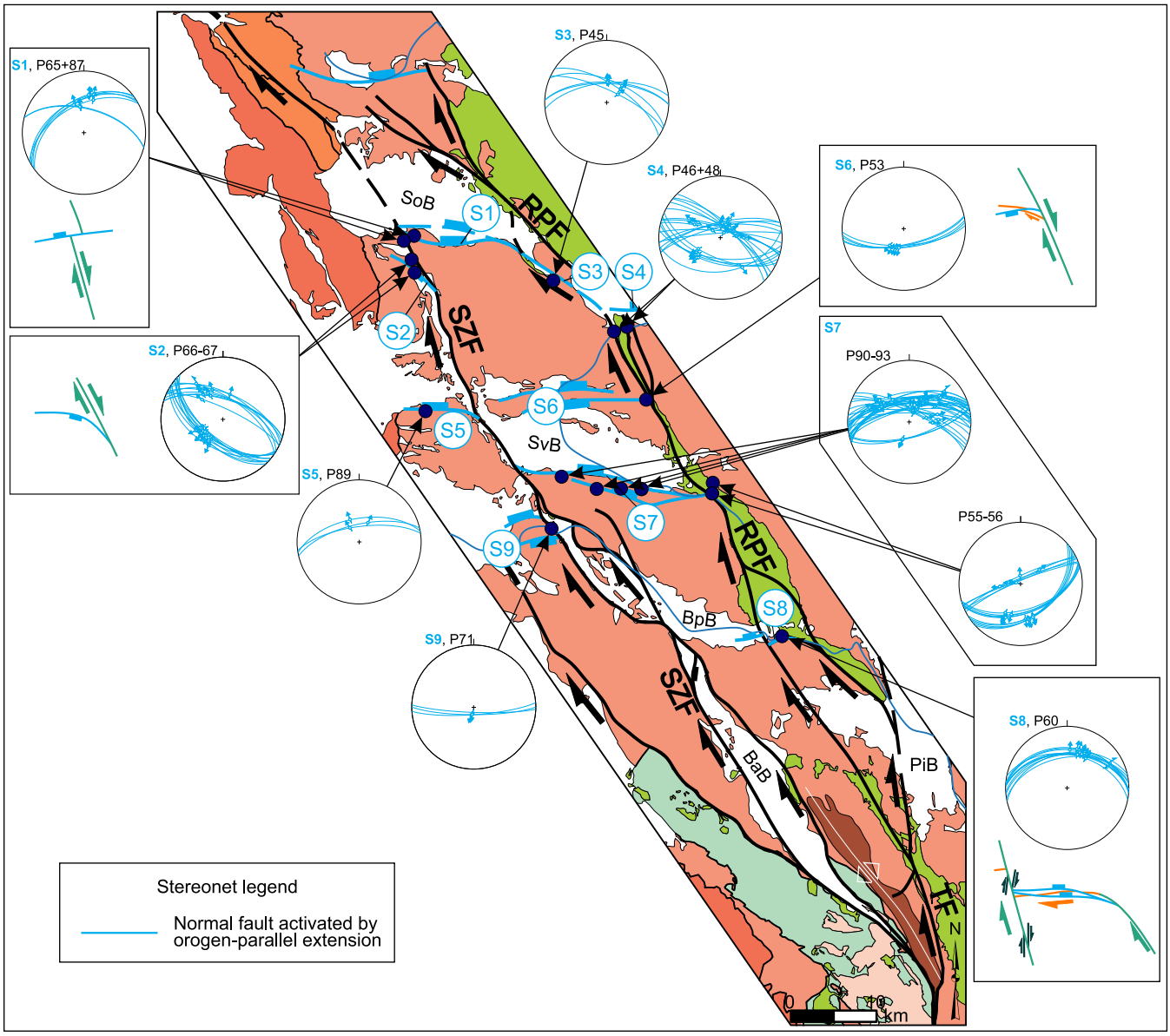

Fig. 8. Structural map and lower hemisphere stereographic projections of faults associated with orogen-parallel extension and Neogene basin formation. The location of the map is displayed in Fig. 2. Faults covered by Neogene sediments or faults with unclear prolongation are dashed. Numbered structures in stereonets correspond to map-scale structures with the same number. Each structure may combine multiple observation points. S - structure; P - observation point. Faults measured in the outcrops are located within or correlated with faults at map-scale with the same kinematics. BaB - Babušnica Basin; BpB - Bela Palanka Basin; PiB - Pirot Basin; RPF - Rtanj-Pirot Fault; SZF - Sokobanja-Zvonce Fault; SoB - Sokobanja Basin; SvB - Svrljig Basin; TF - Timok Fault.

4.3. E-W oriented normal faults

Outside the main strike-slip fault zones, the Rtanj-Pirot and Sokobanja-Zvonce Faults are connected by gradually rotating to E-W oriented top-N normal faults that are roughly perpendicular to the orogenic strike (Figs. 2, 6, 8). This is documented by a change in strike and kinematics of faults from dextral NNW-SSE oriented to normal E-W oriented. The normal faults control the sedimentation in the early middle Miocene Sokobanja and Svrljig Basins, while the higher elevation of Paleozoic metasediments in their footwalls indicates exhumation and block-tilting (Figs. 8, 3g). At the outcrop scale, there is a large variability of the observed senses of shear, but in general, both N- and S-dipping conjugated sets of normal faults are observed (Fig. 8). Deformation along these normal faults is characterized by striated fault planes or fault gouges. Their offset increases westwards, closer to the Sokobanja-Zvonce Fault (e.g., Fig. 7g, S1 in Fig. 8), while towards their eastern connection with the Rtanj-Pirot Fault, the deformation is more distributed to a larger number lower offset, often conjugate normal faults (e.g., Fig. 7h, S7 in Fig. 8).

The normal faults often truncate E-W oriented splays of the Rtanj-Pirot and Sokobanja-Zvonce faults (e.g., S6 or S8 in Fig. 8), while they show a mutual cross-cutting relationship with NNW-SSE oriented dextral faults. For instance, normal faults truncate strike-slip faults (e.g., Fig. 7g, S2 in Fig. 6 and S1 in Fig. 8), but the opposite is also observed either by truncation or by a gradual clockwise rotation of normal faults when approaching a dextral strike-slip corridor (e.g., S2, Fig. 8). This mutual interplay between normal and dextral strike-slip faulting demonstrate that they formed during the same deformation event.

5. Summary and integration of outcrop- and map-scale structures in the context of strain partitioning

The dominant strike-slip deformation observed on the outcrop scale is in agreement with the regional structure, which shows large offset dextral faults (Figs. 2 and 3). These faults include the previously known Cerna and Timok Faults, but also the lower offset dextral, newly discovered Sokobanja-Zvonce and Rtanj-Pirot Faults, as well as numerous other similarly oriented smaller faults (Figs. 4 and 6). All these structures cross-cut the Cretaceous nappe-stack of the Carpatho-Balkanides orocline, including the Danubian nappes, and part of the adjacent Balkanides (Figs. 2 and 3). Typically, these large strike-slip faults are composed of multiple fault strands (e.g., area of Iron Gates gorge, between the Timok and Knjaževac Basins, NNW of the Pirot Basin or along the Babušnica Basin margins, Figs. 4, 6). Fault strands are often connected by splaying, branching or truncations.

In the north, transtensional deformation created large-scale negative flower structures along the Cerna and Timok Faults (Figs. 3a, b), opening the middle Miocene Donji Milanovac and Orşova intramontane basins (along Cerna) and the early – middle Miocene Timok and Knjaževac Basins (along the Timok Fault, Figs. 2, 4). In the latter, oblique normal faults likely root in the main Timok strike-slip strand in the subsurface (Figs. 2, 3c and 4). Subsidence in these basins reaches a maximum near the Timok Fault, where more than 1.5 km thick sediments are observed (Marović et al., 2007). Southwards, the NNW-SSE oriented segments of the Cerna and Timok Faults (bounding the Deli Jovan and Zaglavak ophiolites, respectively, in Fig. 2) dip ENE-wards and have similar kinematics (Fig. 4, compare Cerna Fault in Fig. 3b with Timok Fault in Fig. 3d). This observation suggests that the Cerna Fault and the southern segment of the Timok Fault made up the same fault prior to the 65 km dextral offset of the Timok northern segment.

The decrease in dextral offset from 65 km in the area of the Zaglavak ophiolite to 8 km south of the Pirot Basin is partly accommodated by the transfer of Timok strike-slip deformation to thrusting in the Balkanides (Figs. 2 and 4). Outcrop-scale fault kinematics document this transfer immediately north of the Pirot Basin where dextral and reverse oblique faulting gradually changes to thrusting and internal folding of the frontal Getic nappe in the Balkanides, with cumulative shortening in the order of less than 10 km (Figs. 3e, f). The remaining dextral offset is too large to be accommodated by other dextral faults and the orogen-parallel extension (see below). Therefore, we follow previous interpretations (Schmid et al., 2020) and infer that a large part of the Timok dextral offset is transferred to thrusting and deformation inside the West Balkan unit, its frontal thrusting and internal deformation of the Forebalkan unit (Fig. 3c-f). Deformation along the main thrusts has often a dextral component, while their offset increases towards the Timok Fault, where the nappe-stack has a dextral drag-folding geometry, in agreement with outcrop observations (Figs. 2 and 4). A structural projection at the Permo-Triassic level indicates that the internal shortening and frontal thrusting of the West Balkan unit are in the order of up to 20 km, while probably less than 5 km in the Forebalkan unit (Fig. 3e, f). Part of this overall Getic and West Balkan deformation must be late Early Cretaceous in age by the correlation with the Danubian nappes, which is constrained by post-tectonic Upper Cretaceous sediments covering thrust contacts in the vicinity of the basal (frontal) Getic thrusting (Ivanov, 1988; Vangelov et al., 2013; Schmid et al., 2020). However, such overprinting relations are unclear elsewhere in the West Balkan and Forebalkan units.

West of the Timok Fault, a part of the dextral offset is taken up by the dextral Rtanj-Pirot and Sokobanja-Zvonce Faults (Fig. 3c-e), which splay off the Timok Fault in the south (Figs. 2 and 6). The Rtanj-Pirot Fault deforms Late Cretaceous and Paleocene sediments (Figs. 3c-e, 6, 7a-c) and has both transtensive and transpressive kinematics, observed by outcrop- and map-scale positive flower structures (Figs. 6, 7b). The transtensive kinematics is only locally observed at the connection with some of the basins (e.g., Knjaževac and Sokobanja, Figs. 3c and 6), while the transpressive kinematics is always associated with fault bends or with fault splaying and stranding into multiple structures (Fig. 3d, e). Although good map-scale regional offset markers are rare, we estimate the fault offset based on displaced slivers of Upper Cretaceous strata inside fault zones. These displacements accumulate ~10 km of dextral offset in the south (north of the Pirot Basin), which increases northwards to ~15 km in the area between Sokobanja and Svrljig Basins (Figs. 2, 6).

Westwards, the Sokobanja-Zvonce Fault truncates upper Eocene – Oligocene sediments of the Babušnica Basin (Figs. 3e, 6 and 7e). Transtensive kinematics along the fault created along-strike accommodation space for the deposition of early middle Miocene sediments in a narrow corridor along its strike (Figs. 3c, d, and 5). Based on map-scale observations of dextral dragging in the Svrljig and Bela Palanka Basins and associated E-W oriented normal faults, we infer that the Sokobanja-Zvonce Fault accumulates 15–20 km of dextral offset (Figs. 2, 6). To the NNW, offsets at both, the Rtanj-Pirot and the Sokobanja-Zvonce faults decrease where they terminate in horse-tail structures north of the *E*-W oriented Miocene basins (Fig. 2).

Regional E-W oriented normal faults correlate with the outcrop kinematics and can be observed only west of the Timok Fault (Fig. 8). These faults control the early middle Miocene subsidence and deposition in multiple intramontane basins, among which the largest are the Sokobanja and Svrljig Basins (Figs. 3d, g, and 8). These faults often splay close to the surface into multiple sub-parallel faults that root likely into a larger partly listric-geometry normal fault at depth (Fig. 3g). While localized deformation along these normal faults leads to a total vertical offset of up to 2 km (Fig. 3g) in central and western segments, deformation is distributed over a higher number of low-offset faults farther to the east, resulting in the narrowing of basins in the same direction (Fig. 8). These *E*-W oriented normal faults connect with both the Rtanj-Pirot and Sokobanja-Zvonce Faults in map view and outcrops by a gradual change in strike and kinematics from E-W normal to NNW-SSE dextral (Figs. 6, 8). Therefore, we have interpreted that the normal faults connect at depth with these dextral strike-slip faults (Fig. 3c, d). In more details, the normal faults splay from the Rtanj-Pirot Fault or otherwise reactivate its E-W oriented strike-slip splays (Figs. 6, 8) and show a mutual cross-cutting relationship with the Sokobanja-Zvonce Fault

where they are also dragged in dextral strike-slip corridors (Figs. 6, 8). The regional E-W oriented normal faults have higher offsets westwards, and they are grouped in half-graben geometries (Sokobanja and Svrljig Basins, Fig. 3d, g, see also Marović et al., 2007). Similarly, this orogen-parallel extension controlled the opening of the Žagubica Basin north of the studied area (Fig. 2). However, normal faults controlling this basin do not demonstrate clear map-scale interaction with dextral strike-slip faults because to the north and northwest of our studied area strike-slip deformation is distributed and rarely localizes along large-offset structures (Krstekanić et al., 2020).

6. Discussion

In summary, our detailed outcrop- and map- scale observations and correlations demonstrate that deformation is differently partitioned west and east of the Cerna-Timok Fault system by a gradual change in kinematics (Fig. 2). To the west, strain is partitioned between the Rtanj-Pirot and Sokobanja-Zvonce strike-slip faults and orogen-parallel extensional structures, where NNW-SSE to NW-SE oriented dextral faults are connected by E-W striking normal faults. Such a connection is counterintuitive for typical stress-inversion approaches when a regional

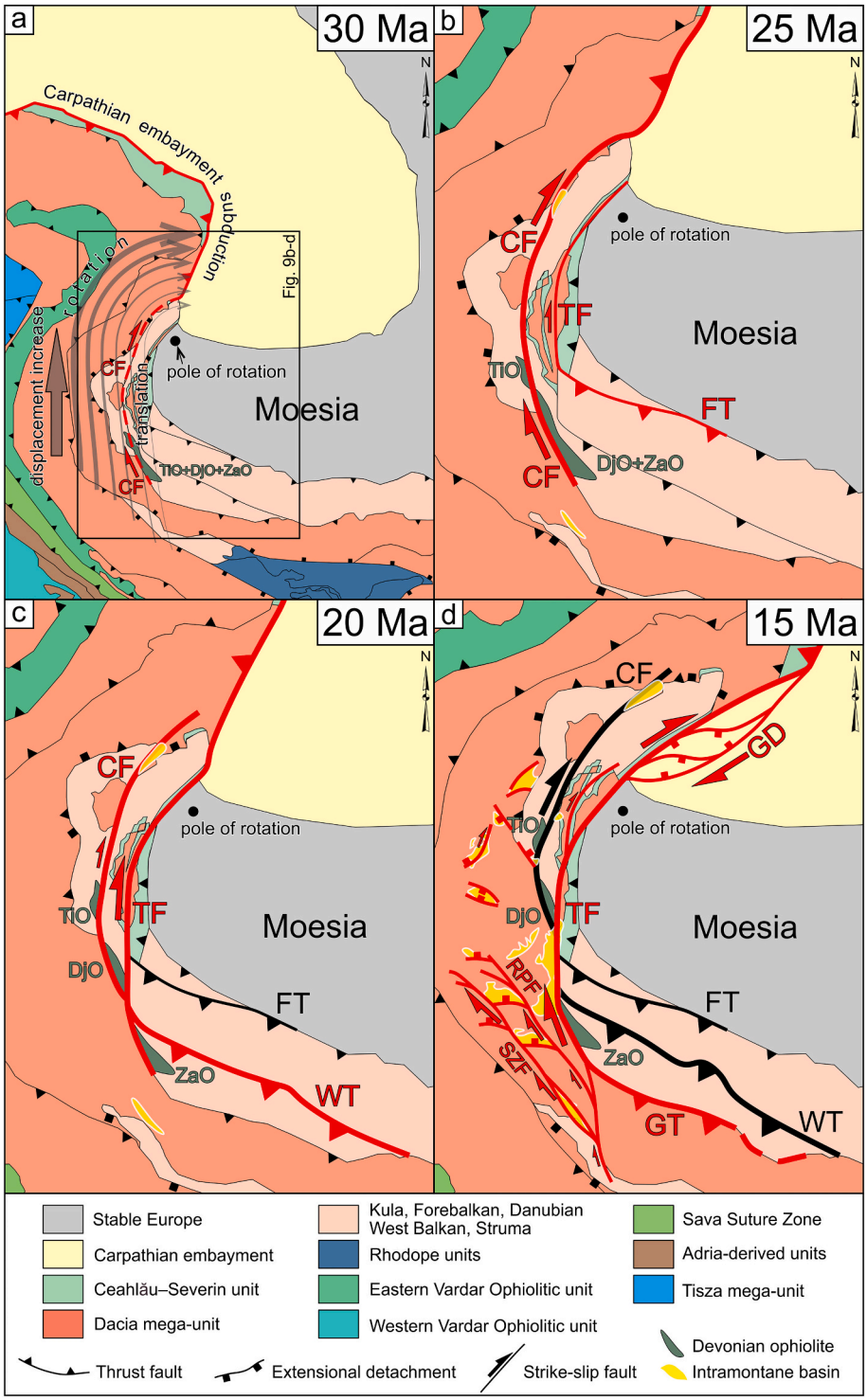

Fig. 9. Quantitative reconstruction with the Circum-Moesian Fault System (CMFS) overlying a detail of a Mediterranean quantitative paleogeographic and geodynamic reconstruction (modified after van Hinsbergen et al., 2020). This is the only reconstruction available where kinematic details of the Carpatho-Balkanides areas are implemented with sufficient details for a quantitative assessment. CF - Cerna Fault; DjO - Deli Jovan ophiolite; FT - Forebalkan Thrust; GD - Getic Depression Basin; GT - Getic Thrust; TF - Timok Fault; TiO - Tisovita-Iuti ophiolite; WT - West Balkan Thrust; ZaO - Zaglavak ophiolite. a) - d) Timesteps of the reconstruction at 30, 25, 20 and 15 Ma. The thickness of the grey arrow lines in a) indicates an increase in the amount of translation and clockwise rotation westwards.

homogenous stress field is applied to map-scale fault kinematics and evolution, and requires a more detailed strain partitioning explanation, detailed in the subsequent sections. To the east and southeast, the Cerna-Timok system transfers a large part of its offset to thrusting in the Balkanides. The timing of this deformation is constrained by cross-cutting relationships, deformation truncating Upper Cretaceous - Paleogene sediments, *syn-* to post- kinematic deposition observed in the early-middle Miocene sediments of the Timok and Knjaževac Basins, middle Miocene of the Donji Milanovac, Orşova, Kučevo, Žagubica, Sokobanja, Svrljig Basins and the narrow middle Miocene corridors along the Sokobanja-Zvonce Fault (Fig. 2). These timing constraints show that deformation was active during post-Eocene and pre-late middle Miocene times. Superposition criteria suggest that deformation started with a deformation transfer from strike-slip to thrusting east of the Cerna-Timok system while being coeval and followed by partitioning between strike-slip and orogen-parallel extension west of the same system.

6.1. The Circum-Moesian Fault System

The Circum-Moesian Fault System is related to the coeval formation of contrasting types of deformation that affected the orogens around the Moesian Platform. In our studied area of the Serbian Carpathians, this system experienced partitioning of the major dextral deformation into laterally continuous structures with different, orogen-parallel extension and thrusting kinematics. This type of strain partitioning can be correlated at a more regional area including the South Carpathians and Balkanides during the gradual Oligocene – middle Miocene formation of the backarc-convex orocline.

North of our studied area, the age of the prolongation of the Cerna Fault is constrained to late Oligocene by the formation of the Petroşani Basin in the South Carpathians (Fig. 1b, Berza and Drăgănescu, 1988; Moser et al., 2005) during the gradual oroclinal bending and dextral splaying demonstrated in the study by Ratschbacher et al. (1993). Our Timok Fault kinematic data and regional observations are also in agreement with the northward early Miocene transtensional formation of the Getic Depression Basin in the South Carpathians foreland, repeatedly reactivated and truncated during the subsequent middle-late Miocene transpressional emplacement over the Moesian Platform (Figs. 1b, 2; Krézsek et al., 2013; Matenco et al., 2003; Rabăgia and Maţenco, 1999). The cessation of transtensional activity along the Timok Fault is demonstrated by middle Miocene sediments (i.e., ~13.4 Ma, middle Badenian in the Eastern Paratethys local stratigraphic division or late Badenian in the Central Paratethys domain) of the Getic Depression, which seal the fault (Matenco et al., 2016).

To the south, the curved geometry and the thrusting offset of the West Balkan unit decrease gradually to zero eastwards, away from the drag-folding effect of the Timok Fault (Fig. 1). At the Balkanides scale, the late Early Cretaceous and Eocene structuration can be demonstrated only for the Getic/Sredna Gora and Forebalkan thrusting, respectively, outside the area of the West Balkan unit (see also Schmid et al., 2020; Vangelov et al., 2013). Therefore, it is likely that the West Balkan unit was emplaced during the CMFS formation by partly transferring the Timok-Cerna dextral offset to thrusting (Fig. 9). There are no further geologic (or geochronologic) constraints available for more precise timing of emplacement of the West Balkans unit in the vicinity of the Timok Fault, but our superposition relationships indicate that the overall eastward transfer of dextral strike-slip to thrusting was initiated earlier than the westward transfer to normal faulting and intramontane basin formation. The remaining ~8 km Timok dextral offset left south of the Pirot Basin disappears southwards in a horse-tail structural geometry (Vangelov et al., 2016). Our data do not confirm the previously speculated south-eastwards connection between the Timok Fault and the Maritsa Fault of the northern Rhodope (details in Schmid et al., 2020), which is also not apparent in available geologic maps (see the 1:50.000 scale maps of the Bulgarian Geological Survey).

6.2. Reconstruction and the influence of the geodynamic driver

Regional data infer that CMFS was active during a period of 15–17 Myr during the late Oligocene – middle Miocene (~30–13.4 Ma). By cumulating the offset of the Cerna, Timok, Rtanj-Pirot and Sokobanja-Zvonce Faults, the total amount of dextral motions accommodating translations and rotations in the studied areas is in the order of 140 km. This allows for calculating an average deformation rate of ~8.23–9.33 mm/yr, which is similar to other large intracontinental strike-slip faults, such as the San Andreas Fault system (Mann, 2007). 140 km of dextral displacement correlates with the amount of shortening recorded by the external thin-skinned nappes of the SE Carpathians (e.g., Ellouz et al., 1994), which started in Oligocene times, as demonstrated by low-temperature thermochronology (Necea et al., 2021). This correlation suggests that the shortening associated with the Carpathians subduction has been directly transferred to the CMFS dextral strike-slip during the formation of the backarc-convex orocline. Note that the amount of shortening gradually increases in the Carpathians north of their SE corner to 180 and 220 km or more (see van Hinsbergen et al., 2020 and references therein), but such an increase is an effect of the clockwise rotation around a pole located in the western Moesian platform (Fig. 9a; the pole of rotation location is estimated after van Hinsbergen et al., 2020 and structural patterns of this study). The same rotational effect implies that deformation increases westwards in our studied area.

The CMFS postdates the Paleocene - Eocene orogen parallel extension recorded by the exhumation of the Danubian units and the coeval thrusting in the Balkanides (Fügenschuh and Schmid, 2005; Matenco and Schmid, 1999; Schmid et al., 1998, 2020; Vangelov et al., 2013). This extensional exhumation is an effect of the same general rotation and translation of the Dacia mega-unit, which was significantly rotated around the Moesian Platform already by the end of Eocene, as shown by large-scale tectonic reconstructions (e.g., Fügenschuh and Schmid, 2005; van Hinsbergen et al., 2020). This observation demonstrates that dextral strike-slip faulting, related to the Moesian indentation, started after the Eocene orogen-parallel extension and Balkanides thrusting, as previously inferred (Ratschbacher et al., 1993). However, the present dataset cannot preclude an earlier Eocene strike-slip precursor of the Cerna or Timok Faults. The described variability in offsets along various segments of strike-slip faults and their transfer to thrusting and normal faulting demonstrate that the late Oligocene 35 km Cerna dextral offset (separating the Tisovita-Iuti from the combined Deli Jovan and Zaglavak ophiolite segments, Fig. 9b) was continued by a larger 65 km Timok offset by shortcutting deformation in an eastward splay (offsetting the Deli Jovan and Zaglavak ophiolite segments, Fig. 9c). In other words, the continuation to the south of the Cerna Fault is represented by the southern part of the Timok Fault, which transfers deformation to the West Balkan thrust system. Possibly, the Timok Fault was also activated during the late Oligocene, but such activation requires deformation transfer to relatively low thrusting offsets in the Balkanides (such as along the Forebalkan Thrust, as suggested in Fig. 9b). The subsequent Miocene Timok dextral offset was transferred mostly to the frontal Getic/Sredna Gora and West Balkan thrust systems and associated internal deformation in the latter (Fig. 9c). It is also clear that dextral dragging of these units (Fig. 1) was created by gradually eastwards decreasing the amount of post-Eocene thrusting.

The ~20 Ma onset of Carpathian slab retreat, recorded by the formation of the Pannonian backarc basin (e.g., Horváth et al., 2015), changed the situation by dramatically increasing the total amount and rates of CMFS dextral deformation during the formation of the backarc-convex orocline, from 35 km pre-roll-back Cerna Fault displacement (rate of ~3.5 mm/yr) to syn-roll-back 100 km offset of the combined Timok, Rtanj-Pirot and Sokobanja-Zvonce (rate of up to ~2 cm/yr). This process is also responsible for the rapid transtensional formation of the Getic Depression Basin in the frontal part of the South Carpathians in the prolongation of the Timok Fault (Krézsek et al., 2013; Rabăgia and Maţenco, 1999). As deformation progresses and increases northwards,

older segments of the Cerna and Timok Faults were bent by the rotation, while truncated by progressively younger NE-SW to E-W oriented dextral faults (such as structure S3, Fig. 4). This gradual rotation continued in the South Carpathians and its frontal Getic Depression, where is truncated by subsequent NW-SE to NNW-SSE oriented late Miocene strike-slip, which is the ultimate expression of dextral faulting accommodating the movement around the Moesian margin during rotation (Hippolyte et al., 1999; Maţenco et al., 1997; Rabăgia et al., 2013; Ratschbacher et al., 1993;).

Correlating the observed structures with the coeval deformation observed to the south and southeast in the Rhodope Mountains is more difficult with data presented in our study, particularly because our mapped prolongation of the Timok Fault south of the Pirot Basin has a minor total offset and appears to terminate southwards in a horse-tail structure. Such a continuation is not required for the post-Cretaceous evolution because of the large-scale strain partitioning between the western Hellenides shortening and the post 42 Ma extension (Rhodope, southern Balkanides and Aegean) associated with the Aegean slab retreat, which has a pole of rotation somewhere near the termination of the Timok Fault (Fig. 1a, Brun and Sokoutis, 2007; Schmid et al., 2020, van Hinsbergen et al., 2020). A SE continuation of the Timok Fault is also prevented by the transfer of deformation to thrusting during indentation, as shown by recent analogue modelling applied to the study area (Krstekanić et al., 2021).

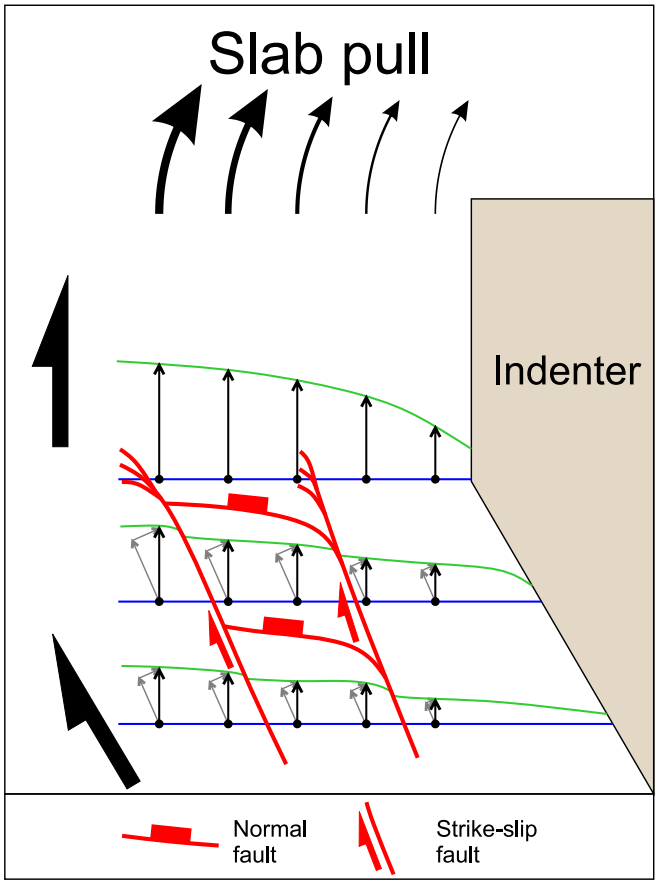

Fig. 10. Map-view sketch of strain partitioning in coupled NNW-SSE strike-slip and N-S (orogen-parallel) extension. Blue and green lines are marker lines, showing the situation before (blue) and after (green) the deformation. Black arrows show displacement variability due to the slab pull. Arrows' size indicates a relative difference in displacement magnitude. Note the increase in displacements westwards and northwards, created by slab pull. Grey arrows are indenter margin-parallel and perpendicular components of displacement. Half arrows indicate overall dextral drag against the indenter. Because displacements increase from south to north, there is an extension in the N-S direction creating E-W oriented normal faults. Strike-slip faults accommodate the abrupt change of indenter margin-parallel component of displacement. When there is a more gradual change in displacements (like along the N-S oriented indenter margin, northernmost marker line), there is no strike-slip faulting. (For interpretation of the references to colour in this figure legend, the reader is referred to the web version of this article.)

6.3. *Mechanism of strain partitioning and similar observations elsewhere*

The post-20 Ma pull exerted by the retreating Carpathian slab and increasing the amount of deformation at farther distances from the pole of rotation was accommodated by orogen-parallel extension and formation of intramontane basins in the Serbian Carpathians (Fig. 9d). In our view, this is a clear expression of strain partitioning, because NW-SE dextral faults cannot form together with E-W oriented normal faults in isotropic materials and homogenous stress field (Fig. 10). Instead, the northward pull on the upper plate exerted by the Carpathian slab combined with the clockwise rotation and drag in respect to the Moesian Platform are creating higher displacements to the north and west (Fig. 10). This change in displacements is accommodated by splaying from the Timok Fault to E-W oriented normal faults accommodating the N-S oriented orogen-parallel extension. In more details, dextral faults terminating in horse-tails are activated successively at a farther distance from the Timok Fault, i.e. first the Rtanj-Pirot Fault, followed by the Sokobanja-Zvonce Fault. The latter truncates the earlier curved fault that shows a transfer of kinematics from NW-SE dextral to E-W normal faulting (Figs. 9d, 10).

The Carpatho-Balkanides backarc-convex orocline was ultimately controlled by the geometry of the Moesian indenter and the Carpathians subduction. Similar situations are observed elsewhere. For instance, the much larger indentation of India shows shortening in the Himalayas (Figs. 11a, b; e.g., Molnar and Tapponier, 1975; Tapponnier et al., 1986) being transferred to a strike-slip deformation that changes strike and ultimately becomes parallel with the margins of the indenter such as in the SE Asia (Morley, 2002, 2013; Morley and Arboit, 2019; Sloan et al., 2017; Vigny et al., 2003), during the coeval backarc-convex oroclinal bending around the Eastern Himalayan Syntaxis (e.g., van Hinsbergen et al., 2019). Although the fault pattern is fairly more complex and is controlled by the inherited structures (Morley, 2007), the facilitators were the northward push by the lower plate Indian indenter and the retreating Sunda subduction pulling the upper plate, Sundaland, with higher velocities closer to the subduction zone (Sternai et al., 2016). The deformation during this gradual oroclinal bending of the initially less curved Eurasian margin (Fig. 11a) around the Indian indenter was partitioned along the large-scale dextral Sagaing Fault at the Indian eastern margin (Fig. 11b). The Sagaing Fault connects the thrusting in the Himalayas and the opening of the pull-apart Andaman Sea Basin above the Sunda subduction zone (Fig. 11b; Morley, 2002, 2013; Sloan et al., 2017), while it separates two regions of deformation transfer. West of the Sagaing Fault (i.e., towards the indenter) the strike-slip is transferred to transpression and thrusting (e.g., Maurin et al., 2010; Nielsen et al., 2004), while the strain is partitioned eastwards between strike-slip and normal faults (Morley, 2007). Therefore, although significantly larger, the mechanism of transfer from shortening in the Himalayas to complex strike-slip deformation along the Sagaing Fault during oroclinal bending around the Eastern Himalayan Syntaxis is comparable to the mechanism of the Balkanides shortening transfer to Cerna and Timok strike-slip deformation during oroclinal bending around the Moesia.

The relative plate motion in cases of the Moesian and Indian indentation and their associated Vrancea and SE Asiaslab retreats are perpendicular to the frontal and parallel to the lateral indenter margins, which results in the large-scale transfer of shortening to strike-slip deformation, while differences in the resulting fault pattern are controlled by the geometry of the two indenters. In the case of India (Fig. 11a, b), the shortening is transferred more abruptly to strike-slip

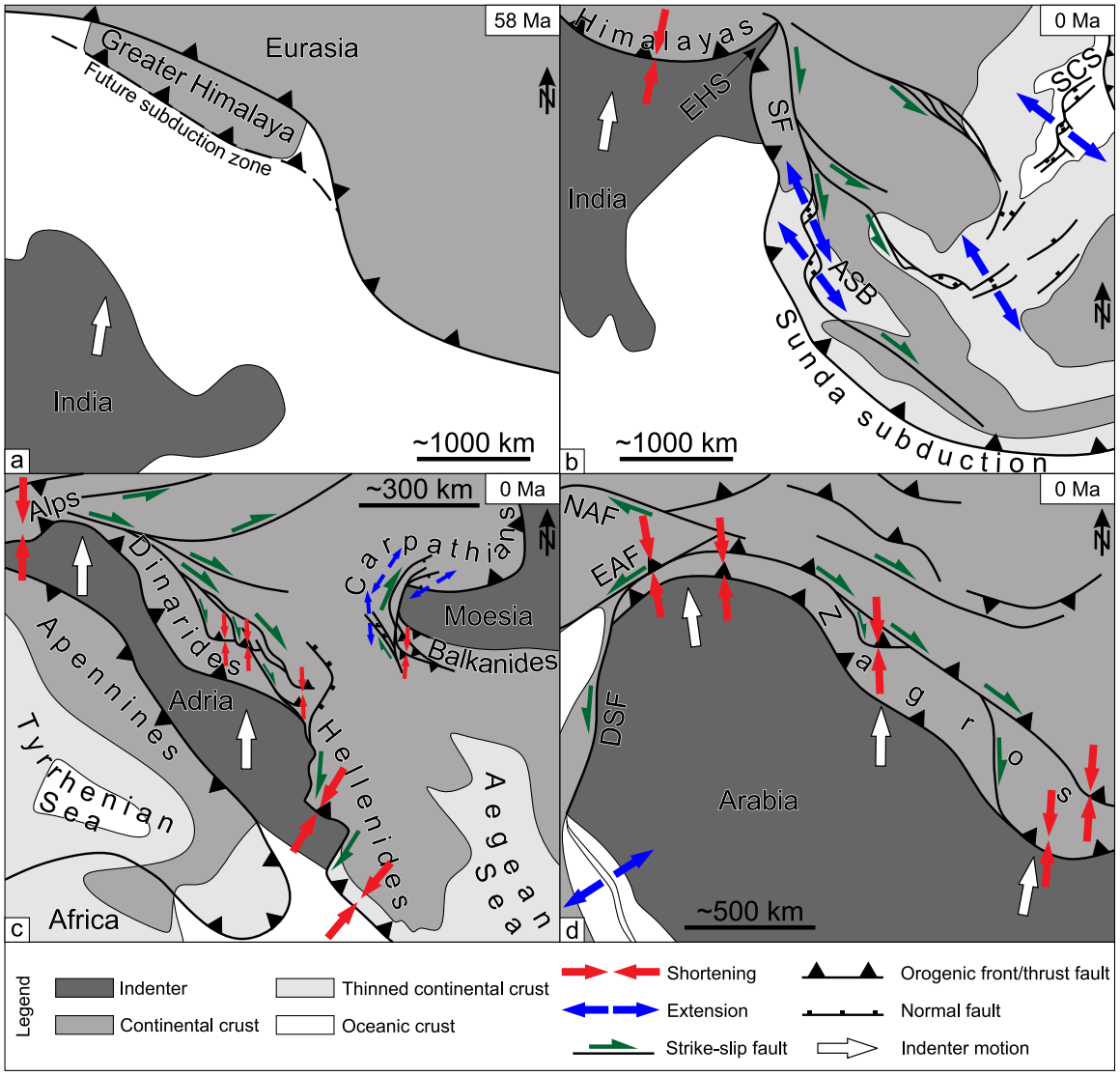

Fig. 11. Sketches of comparative cases of deformation transfer around indenters. a) India – Eurasia tectonic reconstruction in Paleocene (simplified after van Hinsbergen et al., 2019). b) Present-day structure of the India – Eurasia system showing the transfer of deformation around the Indian indenter during indentation and lateral slab roll-back (simplified after Tapponnier et al., 1986; Cullen, 2010; van Hinsbergen et al., 2019). ASB – Andaman Sea Basin; EHS – East Himalayan Syntax; SF – Sagaing Fault. c) Adriatic indentation and transfer of deformation along the Dinarides orogen (simplified after Ratschbacher et al., 1991a; van Unen et al., 2019a; van Hinsbergen et al., 2020). d) Arabian indentation and different styles of deformation transfer along its lateral margins (simplified after Authemayou et al., 2006). DSF – Dead Sea Fault; EAF – East Anatolian Fault; NAF – North Anatolian Fault.

because of the relatively sharp corner in the Eastern Himalayan Syntaxis, while the deformation is transferred more gradually around the Moesian curved southwestern corner (Figs. 1b, 2, 9). In situations when the indenter geometry and relative plate motion are distributed in such a way that the lateral margin of the indenter is oblique to the plate motion, the deformation is transferred from frontal shortening to large-scale transpressive deformation along the oblique lateral indenter margin. Such cases are observed in the Alps transfer of deformation to the Dinarides - Hellenides(Fig. 11c) and in the Zagros (Fig, 11d) orogens along the Adriatic and Arabian oblique eastern margins. In these cases, deformation is partitioned between strike-slip faulting and thrusting in orogen-scale restraining bends or stepovers (e.g., Authemayou et al., 2006; van Unen et al., 2019a). The deformation along the western Arabian margin (Fig. 11d) is accommodated by transpressive East Anatolian Fault (margin oblique to plate motion) and strike-slip to transtensive Dead Sea Fault (margin parallel to plate motion; see Lyberis et al., 1992; Perinçek and Çemen, 1990; Smit et al., 2010).

7. Conclusions

To understand the transfer of deformation during backarc-convex oroclinal bending of the European Carpatho-Balkanides orogen around the Moesian indenter, we have performed a field structural and kinematic study of one of the largest, but poorly documented strike-slip systems known in continental Europe. The results demonstrate that the mechanics of deformation was accommodated by a likely unique situation of complex coeval strike-slip, thrust and normal faults (i.e. by the Circum-Moesian Fault System) that spans a regional area from the South Carpathians to the Balkanides mountains. In the studied region of the Serbian Carpathians, deformation is partitioned to multiple, kinematically different, high-offset faults, that accumulate an offset in the order of 140 km by dextral displacements along the previously known large curved Cerna - Timok system and the newly found Sokobanja-Zvonce and Rtanj-Pirot Faults. These strike-slip faults transfer a significant part of their offset eastwards to thrusting in the Balkanides south of

the Moesian indenter and to an orogen-parallel extension during the formation of intramontane basins westwards. Strike-slip faults often display multi-strand geometries that mutually connect by splaying, branching and truncations, while large faults demonstrate a change in kinematics from dominant transtension in the north to transpression in the south. To the west, the NNW-SSE oriented Sokobanja-Zvonce and Rtanj-Pirot Faults accommodate deformation around the SW Moesian corner, by gradually changing their local strike and connecting or truncating the E-W oriented normal faults that control the formation of intramontane basins, which provide critical timing indicators. These observations demonstrate that the CMFS was active during the late Oligocene – middle Miocene, where dextral deformation progressed at average rates in the order of 9 mm/yr.

The correlation with paleogeographic and geodynamic reconstructions demonstrates that the overall formation of the CMFS system during the indentation of the Moesian Platform was driven by a gradual orogenic translation and rotation during the subduction of the Carpathian embayment. The rotation around the NW corner of the Moesia decreased southwards and was gradually replaced by translation along the Moesian western margin. The ~20 Ma onset of slab retreat and backarc extension has dramatically increased the rates of CMFS dextral deformation from ~3.5 mm/yr to ~2 cm/yr. The pull exerted by the retreating slab has facilitated the transfer of dextral deformation to orogen-parallel extension. The overall strain partitioning mechanics is similar to observations elsewhere, such as in the much larger India – Asia collision zone, but has specific mechanisms of strain partitioning linked to the geometry of the Moesian indenter. This specificity relates to shortcutting the dextral deformation along the margins towards the indenter and the interplay between the gradual activation of strike-slip and orogen-parallel extension.

The results of our study demonstrate that in most cases of indentation, a strain partitioning approach is required to understand the observed patterns of deformation, although is not a standardised methodology and requires adaptation to the specificity of kinematic observations and the mechanism of indentation.

Data availability

Measurements, kinematic and structural data obtained in this study are available in Figs. 4, 6 and 8. The full dataset measured in the field is available in the Supplementary Appendix.

Declaration of Competing Interest

The authors declare that they have no known competing financial interests or personal relationships that could have appeared to influence the work reported in this paper.

Acknowledgements

This paper is part of a collaboration between the Department of Earth Sciences at Utrecht University, the Netherlands and the Faculty of Mining and Geology, University of Belgrade, Serbia during the PhD of Nemanja Krstekanić and is funded by the Netherlands Research Centre for Integrated Solid Earth Science (ISES). We thank Timotije Tufegdžić for his help during the fieldwork. Djordje Grujic is gratefully acknowledged for helpful discussions and suggestions on an earlier version of the manuscript. We thank Editor Zhengtang Guo and two anonymous reviewers for their constructive comments and suggestions, which have significantly improved the original version of the manuscript.

Appendix A. Supplementary data

Supplementary data to this article can be found online at https://doi.org/10.1016/j.gloplacha.2021.103714.

References

Anđelković, J., Krstić, B., Bogdanović, P., Jadranin, D., Milenković, P., Milošaković, R., Urošević, D., 1977. In: Dimitrijević, D., Dolić, D., Rakić, M.O., Jovanović, Lj, Maslarević, Lj, Marković, B., Divljan, M., Đorđević, M. (Eds.), Explanatory Book for Sheets Pirot and Breznik, Basic Geologic Map of SFRY 1:100.000. Savezni geološki zavod, Belgrade.

Andrić, N., Vogt, K., Matenco, L., Cvetković, V., Cloetingh, S., Gerya, T., 2018. Variability of orogenic magmatism during Mediterranean-style continental collisions: a numerical modelling approach. Gondwana Res. 56, 119–134.

Angelier, J., 1979. Determination of the mean principal directions of stresses for a given fault population. Tectonophysics 56, T17–T26.

Angelier, J., 1989. From orientation to magnitudes in paleostress determinations using fault slip data. J. Struct. Geol. 11 (1/2), 37–50.

Angelier, J., 1994. Fault slip analysis and paleostress reconstruction. In: Hancock, P.L. (Ed.), Continental Deformation. Pergamon Press, Oxford, New York, Seoul, Tokyo, pp. 53–100.

Antić, M.D., Kounov, A., Trivić, B., Wetzel, A., Peytcheva, I., von Quadt, A., 2016a. Alpine thermal events in the central Serbo–Macedonian Massif (southeastern Serbia). Int. J. Earth Sci. 105, 1485–1505.

Antić, M., Peytcheva, I., von Quadt, A., Kounov, A., Trivić, B., Serafimovski, T., Tasev, G., Gerdjikov, I., Wetzel, A., 2016b. Pre-Alpine evolution of a segment of the North-Gondwanan margin: Geochronological and geochemical evidence from the central Serbo–Macedonian Massif. Gondwana Res. 36, 523–544.

Antonijević, I., Veselinović, M., Đorđević, M., Kalenić, M., Krstić, B., Karajičić, Lj, 1970. Explanatory Book for Sheet Žagubica, Basic Geologic Map of SFRY 1:100.000. Savezni geološki zavod, Belgrade.

Argand, E., 1924. La tectonique de l'Asie. In: Conférence faite á Bruxelles., le 10 août 1922. Congrès géologique international (XIIIe session)- Belgique, Jun 1922, Belgique, 171-372.

Authemayou, C., Chardon, D., Bellier, O., Malekzadeh, Z., Shabanian, E., Abbassi, M.R., 2006. Late Cenozoic partitioning of oblique plate convergence in the Zagros fold-and-thrust belt (Iran). Tectonics 25, TC3002. https://doi.org/10.1029/2005TC001860.

Balázs, A., Matenco, L., Magyar, I., Horváth, F., Cloetingh, S., 2016. The link between tectonics and sedimentation in back-arc basins: new genetic constraints from the analysis of the Pannonian Basin. Tectonics 35, 1526–1559.

Balla, Z., 1984. The Carpathian loop and the Pannonian Basin: a kinematic analysis. Geophys. Trans. 30 (4), 313–353.

Balla, Z., 1986. Paleotectonic reconstruction of the Central Alpine-Mediterranean belt for the Neogene. Tectonophysics 127, 213–243.

Balla, Z., 1987. Tertiary palaeomagnetic data for the Carpatho–Pannonian region in the light of Miocene rotation kinematics. Tectonophysics 139, 67–98.

Balla, Z., 1988. On the Origin of the structural pattern of Hungary. Acta Geol. Hung. 31 (1–2), 53–63.

Banješević, M., 2006. Upper Cretaceous Magmatism of the Timok Magmatic Complex. PhD Thesis. University of Belgrade, Belgrade (in Serbian).

Benesh, N.P., Plesch, A., Shaw, J.H., 2014. Geometry, kinematics, and displacement characteristics of tear-fault systems: an example from the deep-water Niger Delta. AAPG Bull. 98 (3), 465–482.

Berza, T., Drăgănescu, A., 1988. The Cerna–Jiu fault system (South Carpathians, Romania), a major Tertiary transcurrent lineament. DS Inst. Geol. Geofiz. 72–73, 43–57.

Berza, T., Kräutner, H.G., Dimitrescu, R., 1983. Nappe structure of the Danubian window of the central South Carpathians. Inst. Geol. Geofiz. 60, 31–34.

Berza, T., Constantinescu, E., Vlad, S.N., 1998. Upper Cretaceous marmatic series and associated mineralisation in the Carpathian–Balkan orogen. Resour. Geol. 48 (4), 291–306.

Bogdanović, P., Rakić, M., 1980. Explanatory Book for Sheets Donji Milanovac, Oršova, Baja de Arama and Turnu Severin, Basic Geologic Map of SFRY 1:100.000. Savezni geološki zavod, Belgrade.

Bokelmann, G., Rodler, F.-A., 2014. Nature of the Vrancea seismic zone (Eastern Carpathians) – new constraints from dispersion of first-arriving P-waves. Earth Planet. Sci. Lett. 390, 59–68.

Brun, J.-P., Sokoutis, D., 2007. Kinematics of the Southern Rhodope Core Complex (North Greece). Int. J. Earth Sci. (Geol. Rundsch) 96, 1079–1099.

Burchfiel, B.C., Nakov, R., 2015. The multiply deformed foreland fold-thrust belt of the Balkan orogen, northern Bulgaria. Geosphere 11 (2), 463–490.

Célérier, B., Etchecopar, A., Bergerat, F., Vergely, P., Arthaud, F., Laurent, P., 2012. Inferring stress from faulting: from early concepts to inverse methods. Tectonophysics 581, 206–219.

Cembrano, J., González, G., Arancibia, G., Ahumada, I., Olivares, V., Herrera, V., 2005. Fault zone development and strain partitioning in an extensional strike-slip duplex: a case study from the Mesozoic Atacama fault system, Northern Chile. Tectonophysics 400, 105–125.

Chen, Z., Burchfiel, B.C., Liu, Y., King, R.W., Royden, L.H., Tang, W., Wang, E., Zhao, J., Zhang, X., 2000. Global Positioning System measurements from eastern Tibet and their implications for India/Eurasia intercontinental deformation. J. Geophys. Res. 105 (B7), 16215–16227.

Ciulavu, M., Ferreiro Mählmann, R., Schmid, S.M., Hofmann, H., Seghedi, A., Frey, M., 2008. Metamorphic evolution of a very low- to low-grade metamorphic core complex (Danubian window) in the South Carpathians. In: Siegesmund, S., Fügenschuh, B., Froitzheim, N. (Eds.), Tectonic Aspects of the Alpine-Dinaride-Carpathian System, vol. 298. Geological Society, London, pp. 281–315. Special Publications.

Codrea, V.A., 2001. Badenian insectivores from Bozovici Basin (Southern Carpathians, Caraş-Severin district). Acta Paleontol. Roman. V 3, 67–75.
Csontos, L., Vörös, A., 2004. Mesozoic plate tectonic reconstruction of the Carpathian region. Palaeogeogr. Palaeoclimatol. Palaeoecol. 210, 1–56.
Csontos, L., Nagymarosy, A., Horváth, F., Kovác, M., 1992. Tertiary evolution of the Intra-Carpathian area: a model. Tectonophysics 208, 221–241.
Cullen, A.B., 2010. Transverse segmentationof the Baram-Balabac Basin. NW Borneo: refining the model of Borneo's tectonic evolution. Pet. Geosci. 16, 3–29.
Dallmeyer, R.D., Neubauer, F., Fritz, H., Mocanu, V., 1998. Variscan vs. Alpine tectonothermal evolution of the South Carpathian orogen: constraints from 40Ar/39Ar ages. Tectonophysics 290, 111–135.
Davy, P., Cobbold, P.R., 1988. Indentation tectonics in nature and experiment, 1. Experiments scaled for gravity. Bull. Geol. Inst. Univ. Uppsala, N.S. 14, 129–141.
de Bruijn, H., Marković, Z., Wessels, W., Milivojević, M., van de Weerd, A.A., 2018. Rodent faunas from the Paleogene of south-east Serbia. Palaeobiodivers. Palaeoenviron. 98 (3), 441–458.
de Leeuw, A., Filipescu, S., Maţenco, L., Krijgsman, W., Kuiper, K., Stoica, M., 2013. Paleomagnetic and chronostratigraphic constraints on the Middle to Late Miocene evolution of the Transylvanian Basin (Romania): implications for Central Paratethys stratigraphy and emplacement of the Tisza–Dacia plate. Glob. Planet. Chang. 103, 82–98.
De Vicente, G., Regas, R., Muñoz-Martín, A., Van Wees, J.D., Casas-Sáinz, A., Sopeña, A., Sánchez-Moya, P., Arche, A., López-Gómez, J., Oláiz, A., Fernandez Lozano, J., 2009. Oblique strain partitioning and transpression on an inverted rift: the Castilian Branch of the Iberian Chain. Tectonophysics 470, 224–242.
D'el-Rey Silva, L.J.H., de Oliveira, Í.L., Pohren, C.B., Tanizaki, M.L.N., Carneiro, R.C., de Fernandes, G.L.F., Aragão, P.E., 2011. Coeval perpendicular shortenings in the Brasília belt: collision of irregular plate margins leading to oroclinal bending in the Neoproterozoic of central Brazil. J. S. Am. Earth Sci. 32, 1–13.
Dimitrijević, M.D., 1997. Geology of Yugoslavia. Geological Institute, Belgrade.
Djurović, P., Živković, N., 2013. Morphological and hydrological characteristics of the Serbian border zone towards Bulgaria. Glasnik Srpskog geografskog društva 93 (4), 51–69.
Doblas, M., 1998. Slickenside kinematic indicators. Tectonophysics 295, 187–197.
Doglioni, C., Carminati, E., Cuffaro, M., Scrocca, D., 2007. Subduction kinematics and dynamic constraints. Earth Sci. Rev. 83, 125–175.
Dupont-Nivet, G., Vasiliev, I., Langereis, C.G., Krijgsman, W., Panaiotu, C., 2005. Neogene tectonic evolution of the southern and eastern Carpathians constrained by paleomagnetism. Earth Planet. Sci. Lett. 236, 374–387.
Ellouz, N., Roure, F., Săndulescu, M., Badescu, D., 1994. Balanced cross sections in the Eastern Carpathians (Romania): a tool to quantify Neogene dynamics. In: Roure, F., Ellouz, N., Shein, V.S., Skvortsov, I. (Eds.), Geodynamic Evolution of Sedimentary Basins, International Symposium Moskow 1992 Proceedings. Technip, Paris, pp. 305–325.
Erak, D., Matenco, L., Toljić, M., Stojadinović, U., Andriessen, P.A.M., Willingshofer, E., Ducea, M.N., 2017. From nappe stacking to extensional detachments at the contact between the Carpathians and Dinarides – the Jastrebac Mountains of Central Serbia. Tectonophysics 710–711, 162–183.
Faccenna, C., Becker, T.W., Auer, L., Billi, A., Boschi, L., Brun, J.P., Capitanio, F.A., Funiciello, F., Horvàth, F., Jolivet, L., Piromallo, C., Royden, L., Rossetti, F., Serpelloni, E., 2014. Mantle dynamics in the Mediterranean. Rev. Geophys. 52, 283–332.
Frisch, W., Kuhlemann, J., Dunkl, I., Brügel, A., 1998. Palinspastic reconstruction and topographic evolution of the Eastern Alps during late Tertiary tectonic extrusion. Tectonophysics 297, 1–15.
Fügenschuh, B., Schmid, S.M., 2005. Age and significance of core complex formation in a very curved orogen: evidence from fission track studies in the South Carpathians (Romania). Tectonophysics 404, 33–53.
Gallhofer, D., von Quadt, A., Peytcheva, I., Schmid, S.M., Heinrich, C.A., 2015. Tectonic, magmatic, and metallogenic evolution of the Late Cretaceous arc in the Carpathian–Balkan orogen. Tectonics 34, 1813–1836.
Glen, J.M.G., 2004. A kinematic model for the southern Alaska orocline based on regional fault patterns. In: Sussman, A.J., Weil, A.B. (Eds.), Orogenic Curvature: Integrating Paleomagnetic and Structural Analyses: Geological Society of America Special Paper 383. Geological Society of America, Boulder, CO, pp. 161–172.
Grădinaru, M., Lazar, I., Bucur, I.I., Grădinaru, E., Săsăran, E., Ducea, M.N., Andrăşanu, et al., 2016. The Valanginian history of the eastern part of the Getic Carbonate Platform (Southern Carpathians, Romania): evidence for emergence and drowning of the platform. Cretac. Res. 66, 11–42.
Hippolyte, J.-C., Badescu, D., Constantin, P., 1999. Evolution of the transport direction of the Carpathian belt during its collision with the east European Platform. Tectonics 18 (6), 1120–1138.
Hippolyte, J.-C., Bergerat, F., Gordon, M.B., Bellier, O., Espurt, N., 2012. Keys and pitfalls in mesoscale fault analysis and paleostress reconstructions, the use of Angelier's methods. Tectonophysics 581, 144–162.
Hír, J., Venczel, M., Codrea, V., Angelone, C., van den Hoek Otende, L.W., Kirscher, U., Prieto, J., 2016. Badenian and Sarmatian s.str. from the Carpathian area: Overview and ongoing research on Hungarian and Romanian small vertebrate evolution. Comp. Rend. Palevol. 15, 863–875.
Horváth, F., Bada, G., Szafián, P., Tari, G., Ádám, A., Cloetingh, S., 2006. Formation and deformation of the Pannonian Basin: constraints from observational data. Geol. Soc. Lond. Mem. 32, 191–206.
Horváth, F., Musitz, B., Balázs, A., Végh, A., Uhrin, A., Nádor, A., Koroknai, B., Pap, N., Tóth, T., Wórum, G., 2015. Evolution of the Pannonian basin and its geothermal resources. Geothermics 53, 328–352.
Iancu, V., Berza, T., Seghedi, A., Gheuca, I., Hann, H.-P., 2005a. Alpine polyphase tectono-metamorphic evolution of the South Carpathians: a new overview. Tectonophysics 410, 337–365.
Iancu, V., Berza, T., Seghedi, A., Maruntiu, M., 2005b. Paleozoic rock assemblages incorporated in the South Carpathian Alpine thrust belt (Romania and Serbia): a review. Geol. Belg. 8 (4), 48–68.
Ivanov, Ž., 1988. Apercu general sur l'evolution geologique et structurale du massif des Rhodopes dans le cadre des Balkanides. Bull. Soc. Geol. Fr. 4, 227–240.
Johnson, M.R.W., 2002. Shortening budgets and the role of continental subduction during the India–Asia collision. Earth Sci. Rev. 59, 101–123.
Jolivet, L., Faccenna, C., Becker, T., Tesauro, M., Sternai, P., Bouilhol, P., 2018. Mantle flow and deforming continents: from India-Asia convergence to Pacific subduction. Tectonics 37, 2887–2914.
Jones, R.R., Tanner, P.W.G., 1995. Strain partitioning in transpression zones. J. Struct. Geol. 17 (6), 793–802.
Jovanović, D., Cvetković, V., Erić, S., Kostić, B., Peytcheva, I., Šarić, K., 2019. Variscan granitoids of the East Serbian Carpatho-Balkanides: new insight inferred from U–Pb zircon ages and geochemical data. Swiss J. Geosci. 112, 121–142.
Kalenić, M., Đorđević, M., Krstić, B., Bogdanović, P., Milošaković, R., Divljan, M., Čičulić, M., Džodžo, R., Rudolf, Lj, Jovanović, Lj, 1976. Explanatory Book for Sheet Bor, Basic Geologic Map of SFRY 1:100.000. Savezni geološki zavod, Belgrade.
Kalenić, M., Hadži-Vuković, M., Dolić, D., Lončarević, Č., Rakić, M.O., 1980. Explanatory Book for Sheet Kučevo, Basic Geologic Map of SFRY 1:100.000. Savezni geološki zavod, Belgrade.
Kaymakci, N., Inceöz, M., Ertepinar, P., Koç, A., 2010. Late Cretaceous to recent kinematics of SE Anatolia (Turkey). In: Sosson, M., Kaymakci, N., Stephenson, R.A., Bergerat, F., Starostenko, V. (Eds.), Sedimentary Basin Tectonics From the Black Sea and Caucasus to the Arabian Platform, vol. 340. Geological Society, London, pp. 409–435. Special Publications.
Knaak, M., Márton, I., Tosdal, R.M., van der Toorn, J., Davidović, D., Strmbanović, I., Zdravković, M., Živanović, J., Hasson, S., 2016. Geologic Setting and Tectonic Evolution of Porphyry Cu-Au, Polymetallic Replacement, and Sedimentary Rock-hosted Au Deposits in the Northwestern Area of the Timok Magmatic Complex, Serbia, 19. Society of Economic Geologists, pp. 1–28. Special Publication.
Kolb, M., von Quadt, A., Peytcheva, I., Heinrich, C.A., Fowler, S.J., Cvetković, V., 2013. Adakite-like and normal arc magmas: distinct fractionation paths in the East Serbian Segment of the Balkan–Carpathian Arc. J. Petrol. 54 (3), 421–451.
Kräutner, H.G., Krstić, B., 2002. Alpine and Pre-Alpine structural units within Southern Carpathians and the Eastern Balkanides. In: Proceedings of XVII Congress of Carpathian–Balkan Geological Association. Geologica Carpathica, p. 53 (Special Issue).
Kräutner, H.G., Krstić, B., 2003. Geological Map of the Carpatho–Balkanides Between Mehadia, Oraviţa, Niš and Sofia. Geoinstitute, Belgrade.
Krézsek, C., Lăpădat, A., Maţenco, L., Arnberger, K., Barbu, V., Olaru, R., 2013. Strain partitioning at orogenic contacts during rotation, strike-slip and oblique convergence: paleogene–Early Miocene evolution of the contact between the South Carpathians and Moesia. Glob. Planet. Chang. 103, 63–81.
Krstekanić, N., Matenco, L., Toljić, M., Mandic, O., Stojadinovic, U., Willingshofer, E., 2020. Understanding partitioning of deformation in highly arcuate orogenic systems: inferences from the evolution of the Serbian Carpathians. Glob. Planet. Chang. 195, 103361 https://doi.org/10.1016/j.gloplacha.2020.103361.
Krstekanić, N., Willingshofer, E., Broerse, T., Matenco, L., Toljić, M., Stojadinovic, U., 2021. Analogue modelling of strain partitioning along a curved strike-slip fault system during backarc-convex orocline formation: implications for the Cerna-Timok fault system of the Carpatho-Balkanides. J. Struct. Geol. 149, 104386 https://doi.org/10.1016/j.jsg.2021.104386.
Krstić, B., Kalenić, M., Divljan, M., Maslarević, Lj, Đorđević, M., Dolić, D., Antonijević, I., 1976. Explanatory Book for Sheets Knjaževac and Belogradčik, Basic Geologic Map of SFRY 1:100.000. Savezni geološki zavod, Belgrade.
Krstić, N., Savić, Lj, Jovanović, G., 2012. The Neogene Lakes on the Balkan Land. Geološki anali Balkanskog poluostrva, pp. 37–60.
Lacombe, O., 2012. Do fault slip data inversions actually yield "paleostresses" that can be compared with contemporary stresses? A critical discussion. Compt. Rendus Geosci. 344, 159–173.
Lazarević, Z., Milivojević, J., 2010. Early Miocene flora of the intramontane Žagubica Basin (Serbian Carpatho–Balkanides). N. Jb. Geol. Paläont. (Abh.) 256 (2), 141–150.
Lesić, V., Márton, E., Gajić, V., Jovanović, D., Cvetkov, V., 2019. Clockwise vertical-axis rotation in the West Vardar zone of Serbia: tectonic implications. Swiss J. Geosci. 112, 199–215.
Livani, M., Scrocca, D., Arecco, P., Doglioni, C., 2018. Structural and stratigraphic control on salient and recess development along a thrust belt front: the Northern Apennines (Po Plain, Italy). J. Geophys. Res. 123, 4360–4387.
Lyberis, N., Yurur, T., Chorowicz, J., Kasapoglu, E., Gundogdu, N., 1992. The East Anatolian Fault: an oblique collisional belt. Tectonophysics 204, 1–15.
Mai, D.H., 1995. Tertiäre Vegetationsgeschichte Europas. Methoden und Ergebnisse. Gustav Fischer Verlag, Jena, Stuttgart, New York.
Mann, P., 2007. Global Catalogue, Classification and Tectonic Origins of Restraining and Releasing Bends on Active and Ancient Strike-slip Fault Systems, 290. Geological Scociety, London, pp. 13–142. Special Publications.
Mantovani, E., Viti, M., Babbucci, D., Tamburelli, C., Albarello, D., 2006. Geodynamic connection between the indentation of Arabia and the Neogene tectonics of the central–eastern Mediterranean region. In: Dilek, Y., Pavlides, S. (Eds.), Postcollisional Tectonics and Magmatism in the Mediterranean Region and Asia: Geological Society of America Special Paper, 409, pp. 15–41.
Marković, Z., 2003. The Miocene small mammals of Serbia, a review. Deinsea 10, 393–398.

Marković, Z., Wessels, W., van de Weerd, A.A., de Bruijn, H., 2017. On a new diatomyid (Rodentia, Mammalia) from the Paleogene of south-east Serbia, the first record of the family in Europe. Palaeobiodivers. Palaeoenviron. 98 (3), 459–469.
Marović, M., Toljić, M., Rundić, Lj, Milivojević, J., 2007. Neoalpine Tectonics of Serbia. Serbian Geological Society, Belgrade.
Marshak, S., 1988. Kinematics of orocline and arc formation in thin-skinned orogens. Tectonics 7, 73–86.
Martinod, J., Hatzfeld, D., Brun, J.P., Davy, P., Gautier, P., 2000. Continental collision, gravity spreading, and kinematics of Aegea and Anatolia. Tectonics 19 (2), 290–299.
Márton, E., 2000. The Tisza megatectonic unit in the light of paleomagnetic data. Acta Geol. Hung. 43 (3), 329–343.
Maţenco, L., 2017. Tectonics and exhumation of Romanian Carpathians: inferences from kinematic and thermochronological studies. In: Rădoane, M., Vespremeanu-Stroe, A. (Eds.), Landform Dynamics and Evolution in Romania, Springer Geography. Springer, pp. 15–56.
Matenco, L., Radivojević, D., 2012. On the formation and evolution of the Pannonian Basin: constraints derived from the structure of the junction area between the Carpathians and Dinarides. Tectonics 31, TC6007. https://doi.org/10.1029/2012TC003206.
Matenco, L., Schmid, S., 1999. Exhumation of the Danubian nappes system (South Carpathians) during the Early Tertiary: inferences from kinematic and paleostress analysis at the Getic/Danubian nappes contact. Tectonophysics 314, 401–422.
Maţenco, L., Bertotti, G., Dinu, C., Cloetingh, S., 1997. Tertiary tectonic evolution of the external South Carpathians and the adjacent Moesian platform (Romania). Tectonics 16 (6), 896–911.
Matenco, L., Bertotti, G., Cloetingh, S., Dinu, C., 2003. Subsidence analysis and tectonic evolution of the external Carpathian–Moesian Platform region during Neogene times. Sediment. Geol. 156, 71–94.
Matenco, L., Munteanu, I., ter Borgh, M., Stanica, A., Tilita, M., Lericolais, G., Dinu, C., Oaie, G., 2016. The interplay between tectonics, sediment dynamics and gateways evolution in the Danube system from the Pannonian Basin to the western Black Sea. Sci. Total Environ. 543, 807–827.
Maurin, T., Masson, F., Rangin, C., Min, U.T., Collard, P., 2010. First global positioning system results in northern Myanmar: constant and localized slip rate along the Sagaing fault. Geology 38 (7), 591–594.
McKenzie, D., 1972. Active tectonics of the mediterranean region. Geophys. J. R. 30, 109–185.
Melinte-Dobrinescu, M.-C., Jipa, D.C., 2007. Stratigraphy of the Lower Cretaceous sediments from the Carpathian Bend Area, Romania. Acta Geol. Sin. 81 (6), 949–956.
Miser, H.D., 1932. Oklahoma structural salient of the Ouachita Mountains. Geol. Soc. Am. Bull. 43, 138.
Mladenović, A., Antić, M.D., Trivić, B., Cvetković, V., 2019. Investigating distant effects of the Moesian promontory: brittle tectonics along the western boundary of the Getic unit (East Serbia). Swiss J. Geosci. 112, 143–161.
Molnar, P., Tapponier, P., 1975. Cenozoic tectonics of Asia: effects of a continental collision. Science 189 (4201), 419–426.
Morley, C.K., 2002. A tectonic model for the Tertiary evolution of strike–slip faults and rift basins in SE Asia. Tectonophysics 347, 189–215.
Morley, C.K., 2007. Variations in Late Cenozoic–Recent strike-slip and oblique-extensional geometries, within Indochina: the influence of pre-existing fabrics. J. Struct. Geol. 29, 36–58.
Morley, C.K., 2013. Discussion of tectonic models for Cenozoic strike-slip fault-affected continental margins of mainland SE Asia. J. Asian Earth Sci. 76, 137–151.
Morley, C.K., Arboit, F., 2019. Dating the onset of motion on the Sagaing fault: evidence from detrital zircon and titanite U-Pb geochronology from the North Minwun Basin, Myanmar. Geology 47, 581–585.
Moser, F., Hann, H.P., Dunkl, I., Frisch, W., 2005. Exhumation and relief history of the Southern Carpathians (Romania) as evaluated from apatite fission track chronology in crystalline basement and intramontane sedimentary rocks. Int. J. Earth Sci. 94, 218–230.
Necea, D., Juez-Larré, J., Matenco, L., Andriessen, P.A.M., Dinu, C., 2021. Foreland migration of orogenic exhumation during nappe stacking: inferences from a high-resolution thermochronological profile over the Southeast Carpathians. Glob. Planet. Chang. 200, 103457.
Neubauer, F., 2015. Cretaceous tectonics in Eastern Alps, Carpathians and Dinarides: two step microplate collision and Andean-type magmatic arc associated with orogenic collapse. Rend. Online Soc. Geol. Ital. 37, 40–43.
Neubauer, F., Bojar, A.-V., 2013. Origin of sediments during Cretaceous continent-continent collision in the Romanian South Carpathians: preliminary constraints from 40Ar/39Ar single-grain dating of detrital white mica. Geol. Carpath. 56 (5), 375–382.
Neubauer, F., Fritz, H., Genser, J., Kurz, W., Nemes, F., Wallbrecher, E., Wang, X., Willingshofer, E., 2000. Structural evolution within an extruding wedge: model and application to the Alpine-Pannonian system. In: Lehner, F.K., Urai, J.L. (Eds.), Aspects of Tectonic Faulting (Festschrift in Honour of Georg Mandl). Springer-Verlag, Berlin – Heidelberg – New York, pp. 141–153.
Nielsen, C., Chamot-Rooke, N., Rangin, C., the ANDAMAN Cruise Team, 2004. From partial to full strain partitioning along the Indo-Burmese hyper-oblique subduction. Mar. Geol. 209, 303–327.
Obradović, J., Vasić, N., 2007. Jezerski baseni u neogenu Srbije. Special Issues, vol. 662. Serbian Academy of Sciences and Arts, Belgrade.
Orife, T., Lisle, R.J., 2003. Numerical processing of palaeostress results. J. Struct. Geol. 25, 949–957.
Pamić, J., 2002. The Sava-Vardar Zone of the Dinarides and Hellenides versus the Vardar Ocean. Eclogae Geol. Helv. 95, 99–113.
Panaiotu, C.G., Panaiotu, C.E., 2010. Palaeomagnetism of the Upper Cretaceous Sânpetru Formation (Haţeg Basin, South Carpathians). Palaeogeogr. Palaeoclimatol. Palaeoecol. 293, 343–352.
Pătraşcu, S., Bleahu, M., Panaiotu, C., 1990. Tectonic implications of paleomagnetic research into Upper Cretaceous magmatic rocks in the Apuseni Mountains, Romania. Tectonophysics 180, 309–322.
Pătraşcu, S., Bleahu, M., Panaiotu, C., Panaiotu, C.E., 1992. The paleomagnetism of the Upper Cretaceous magmatic rocks in the Banat area of the South Carpathians: tectonic implications. Tectonophysics 213, 341–352.
Pătraşcu, S., Şeclăman, M., Panaiotu, C., 1993. Tectonic implications of paleomagnetism in Upper Cretaceous deposits in the Haţeg and Rusca Montană basins (South Carpathians, Romania). Cretac. Res. 14, 255–264.
Pătraşcu, S., Panaiotu, C., Şeclăman, M., Panaiotu, C.E., 1994. Timing of rotational motion of Apuseni Mountains (Romania): paleomagnetic data from Tertiary magmatic rocks. Tectonophysics 233, 163–176.
Perinçek, D., Çemen, İ., 1990. The structural relationship between the East Anatolian and Dead Sea fault zones in southeastern Turkey. Tectonophysics 172, 331–340.
Petković, K. (Ed.), 1975a. Geologija Srbije: Stratigrafija – prekambrijum i paleozoik. Faculty of Mining and Geology, Belgrade.
Petković, K. (Ed.), 1975b. Geologija Srbije: Stratigrafija – Mezozoik. Faculty of Mining and Geology, Belgrade.
Petrović, B., Dimitrijević, M., Karamata, S., 1973. Explanatory Book for Sheet Vlasotince, Basic Geologic Map of SFRY 1:100.000. Savezni Geološki Zavod, Belgrade.
Plissart, G., Monnier, C., Diot, H., Mărunţiu, M., Berger, J., Triantafyllou, A., 2017. Petrology, geochemistry and Sm-Nd analyses on the Balkan-Carpathian Ophiolite (BCO – Romania, Serbia, Bulgaria): remnants of a Devonian back-arc basin in the easternmost part of the Variscan domain. J. Geodyn. 105, 27–50.
Rabăgia, T., Maţenco, L., 1999. Tertiary tectonic and sedimentological evolution of the South Carpathians foredeep: tectonic vs eustatic control. Mar. Pet. Geol. 16, 719–740.
Rabăgia, T., Matenco, L., Cloetingh, S., 2013. The interplay between eustacy, tectonics and surface processes during the growth of a fault-related structure as derived from sequence stratigraphy: the Govora–Ocnele Mari antiform, South Carpathians. Tectonophysics 502, 196–220.
Ratschbacher, L., Merle, O., Davy, P., Cobbold, P., 1991a. Lateral extrusion in the eastern Alps, part 1: Boundary conditions and experiments scaled for gravity. Tectonics 10 (2), 245–256.
Ratschbacher, L., Frisch, W., Linzer, H.-G., Merle, O., 1991b. Lateral extrusion in the eastern Alps, part 2: Structural analysis. Tectonics 10 (2), 257–271.
Ratschbacher, L., Linzer, H.G., Moser, F., Strusievicz, R.O., Bedelean, H., Har, N., Mogos, P.A., 1993. Cretaceous to Miocene thrusting and wrenching along the central South Carpathians due to a corner effect during collision and orocline formation. Tectonics 12, 855–873.
Regard, V., Faccenna, C., Martinod, J., Bellier, O., 2005. Slab pull and indentation tectonics: insights from 3D laboratory experiments. Phys. Earth Planet. Inter. 149, 99–113.
Rosenberg, C.L., Schneider, S., Scharf, A., Bertrand, A., Hammerschmidt, K., Rabaute, A., Brun, J.-P., 2018. Relating collisional kinematics to exhumation processes in the Eastern Alps. Earth Sci. Rev. 176, 311–344.
Rundić, Lj, Vasić, N., Banješević, M., Prelević, D., Gajić, V., Kostić, B., Stefanović, J., 2019. Facies analyses, biostratigraphy and radiometric dating of the Lower-Middle Miocene succession near Zaječar (Dacian basin, eastern Serbia). Ann. Géol. Péninsule Balkanique 80 (2), 13–37.
Săndulescu, M. (Ed.), 1984. Geotectonica României (Translated Title: Geotectonics of Romania). Tehnică, Bucharest.
Săndulescu, M., 1988. Cenozoic Tectonic history of the Carpathians. In: Royden, L.H., Horvath, F. (Eds.), The Pannonian Basin, A Study in Basin Evolution, AAPG Memoir, vol. 45. American Association of Petroleum Geologists, Tulsa, OK, pp. 17–25.
Sant, K., Mandic, O., Rundić, Lj, Kuiper, K.F., Krijgsman, W., 2018. Age and evolution of the Serbian Lake System: integrated results from Middle Miocene Lake Popovac. Newsl. Stratigr. 51 (1), 117–143.
Savu, H., Udrescu, C., Neacsu, V., Bratosin, I., Stoian, M., 1985. Origin, geochemistry and tectonic position of the Alpine ophiolites in the Severin nappe (Mehedinti Plateau, Romania). Ofioliti 10 (2/3), 423–440.
Schmid, S.M., Berza, T., Diaconescu, V., Froitzheim, N., Fügenschuh, B., 1998. Orogen-parallel extension in the Southern Carpathians. Tectonophysics 297, 209–228.
Schmid, S.M., Bernoulli, D., Fügenschuh, B., Matenco, L., Schefer, S., Schuster, R., Tischler, M., Ustaszewski, K., 2008. The Alpine–Carpathian–Dinaridic orogenic system: correlation and evolution of tectonic units. Swiss J. Geosci. 101, 139–183.
Schmid, S.M., Fügenschuh, B., Kounov, A., Matenco, L., Nievergelt, P., Oberhänsli, R., Pleuger, J., Schefer, S., Schuster, R., Tomljenović, B., Ustaszewski, K., van Hinsbergen, D.J.J., 2020. Tectonic units of the Alpine collision zone between Eastern Alps and western Turkey. Gondwana Res. 78, 308–374.
Searle, M.P., Elliot, J.R., Phillips, R.J., Chung, S.-L., 2011. Crustal–lithospheric structure and continental extrusion of Tibet. J. Geol. Soc. 168, 633–672.
Seghedi, A., Berza, T., Iancu, V., Mărunţiu, M., Oaie, G., 2005. Neoproterozoic terranes in the Moesian basement and in the Alpine Danubian nappes of the South Carpathians. Geol. Belg. 8 (4), 4–19.
Shen, F., Royden, L.H., Burchfiel, B.C., 2001. Large-scale crustal deformation of the Tibetan Plateau. J. Geophys. Res. 106 (B4), 6793–6816.
Sloan, R.A., Elliot, J.R., Searke, M.P., Morley, C.K., 2017. Active tectonics of Myanmar and the Andaman Sea. In: Barber, A., Khin Zaw, J., Crow, M.J. (Eds.), Myanmar: Geology, Resources and Tectonics, vol. 48. Geological Society, London, pp. 19–52. Memoirs.
Smit, J., Brun, J.-P., Cloetingh, S., Ben-Avraham, Z., 2010. The rift-like structure and asymmetry of the Dead Sea Fault. Earth Planet. Sci. Lett. 290, 74–82.

Sperner, B., Zweigel, P., 2010. A plea for more cauton in fault-slip analysis. Tectonophysics 482, 29–41.
Sternai, P., Avouac, J.-P., Jolivet, L., Faccenna, C., Gerya, T., Becker, T.W., Menant, A., 2016. On the influence of the asthenospheric flow on the tectonics andtopography at a collision-subduction transition zones: comparison with the eastern Tibetan margin. J. Geodyn. 100, 184–197.
Stojadinovic, U., Matenco, L., Andriessen, P.A.M., Toljić, M., Foeken, J.P.T., 2013. The balance between orogenic building and subsequent extension during the Tertiary evolution of the NE Dinarides: constraints from low-temperature thermochronology. Glob. Planet. Chang. 103, 19–38.
Stojadinovic, U., Matenco, L., Andriessen, P., Toljić, M., Rundić, Lj, Ducea, M.N., 2017. Structure and provenance of Late Cretaceous–Miocene sediments located near the NE Dinarides margin: inferences from kinematics of orogenic building and subsequent extensional collapse. Tectonophysics 710–711, 184–204.
Tapponnier, P., Peltzer, G., Aramijo, R., 1986. On the mechanics of the collision between India and Asia. In: Coward, M.P., Ries, A.C. (Eds.), Collision Tectonics, Geological Society Special Publication, vol. 19, pp. 115–157.
Toljić, M., Matenco, L., Ducea, M.N., Stojadinović, U., Milivojević, J., Đerić, N., 2013. The evolution of a key segment in the Europe–Adria collision: the Fruška Gora of northern Serbia. Glob. Planet. Chang. 103, 39–62.
Toljić, M., Matenco, L., Stojadinović, U., Willingshofer, E., Ljubović-Obradović, D., 2018. Understanding fossil fore-arc basins: inferences from the Cretaceous Adria-Europe convergence in the NE Dinarides. Glob. Planet. Chang. 171, 167–184.
Twiss, R.J., Unruh, J.R., 1998. Analysis of fault slip inversions: do they constrain stress or strain rate? J. Geophys. Res. 103 (B6), 12205–12222.
Ustaszewski, K., Schmid, S.M., Fügenschuh, B., Tischler, M., Kissling, E., Spakman, W., 2008. A map-view restoration of the Alpine–Carpathian–Dinaridic system for the Early Miocene. Swiss J. Geosci. 101, 273–294.
Ustaszewski, K., Kounov, A., Schmid, S.M., Schaltegger, U., Krenn, E., Frank, W., Fügenschuh, B., 2010. Evolution of the Adria-Europe plate boundary in the northern Dinarides: from continent-continent collision to back-arc extension. Tectonics 29, TC6017. https://doi.org/10.1029/2010TC002668.
van Gelder, I.E., Matenco, L., Willingshofer, E., Tomljenović, B., Andriessen, P.A.M., Ducea, M.N., Beniest, A., Gruić, A., 2015. The tectonic evolution of a critical segment of the Dinarides-Alps connection: Kinematic and geochronological inferences from the Medvednica Mountains, NE Croatia. Tectonics 34, 1952–1978.
van Gelder, I.E., Willingshofer, E., Andriessen, P.A.M., Schuster, R., Sokoutis, D., 2020. Cooling and vertical motions of crustal wedges prior to, during, and after lateral extrusion in the Eastern Alps: new field kinematic and fission track data from the Mur-Mürz Fault System. Tectonics 39 (e2019TC005754).
van Hinsbergen, D.J.J., Dupont-Nivet, G., Nakov, R., Oud, K., Panaiotu, C., 2008. No significant post-Eocene rotation of the Moesian Platform and Rhodope (Bulgaria): implications for the kinematic evolution of the Carpathian and Aegean arcs. Earth Planet. Sci. Lett. 273, 345–358.
van Hinsbergen, D.J.J., Lippert, P.C., Li, S., Huang, W., Advokaat, E.L., Spakman, W., 2019. Reconstructing Greater India: paleogeographic, kinematic, and geodynamic perspectives. Tectonophysics 760, 69–94.
van Hinsbergen, D.J.J., Torsvik, T.H., Schmid, S.M., Maţenco, L.C., Maffione, M., Vissers, R.L.M., Gürer, D., Spakman, W., 2020. Orogenic architecture of the Mediterranean region and kinematic reconstruction of its tectonic evolution since the Triassic. Gondwana Res. 81, 79–229.
van Unen, M., Matenco, L., Demir, V., Nader, F.H., Darnault, R., Mandic, O., 2019a. Transfer of deformation during indentation: inferences from the post-middle Miocene evolution of the Dinarides. Glob. Planet. Chang. 182, 103027.
van Unen, M., Matenco, L., Nader, F.H., Darnault, R., Mandic, O., Demir, V., 2019b. Kinematics of foreland-vergent crustal accretion: inferences from the dinarides evolution. Tectonics 38, 49–76.
Vangelov, D., Gerdjikov, Y., Kounov, A., Lazarova, A., 2013. The Balkan Fold-Thrust Belt: an overview of the main features. Geol. Balcanica 42 (1–3), 29–47.
Vangelov, D., Pavlova, M., Gerdjikov, I., Kounov, A., 2016. Timok fault and Tertiary strike-slip tectonics in part of western Bulgaria. In: Annual of the University of Mining and Geology "St. Ivan Rilski", 59(1), pp. 112–117.
Veselinović, M., Antonijević, I., Milošaković, R., Mićić, I., Krstić, B., Čićulić, M., Divljan, M., Maslarević, Lj, 1970. Explanatory Book for Sheet Boljevac, Basic Geologic Map of SFRY 1:100.000. Savezni geološki zavod, Belgrade.
Veselinović, M., Divljan, M., Đorđević, M., Kalenić, M., Milošaković, R., Rajčević, D., Popović, R., Rudolf, Lj, 1975. Explanatory Book for Sheet Zaječar, Basic Geologic Map of SFRY 1:100.000. Savezni geološki zavod, Belgrade.
Vigny, C., Socquet, A., Rangin, C., Chamot-Rooke, N., Pubellier, M., Bouin, M.-N., Bertrand, G., Becker, M., 2003. Present-day crustal deformation around Sagaing fault, Myanmar. J. Geophys. Res. 108 (B11), 2533. https://doi.org/10.1029/2002JB001999.
von Quadt, A., Moritz, R., Peytcheva, I., Heinrich, C.A., 2005. 3:Geochronology and geodynamics of Late Cretaceous magmatism and Cu-Au mineralization in the Panagyurishte region of the Apuseni–Banat–Timok–Srednogorie belt, Bulgaria. Ore Geol. Rev. 27, 95–126.
Vujisić, T., Navala, M., Kalenić, M., Krstić, B., Maslarević, Lj, Marković, B., Buković, J., 1980. Explanatory Book for Sheet Bela Palanka, Basic Geologic Map of SFRY 1:100.000. Savezni geološki zavod, Belgrade.
Weil, A.B., Sussman, A.J., 2004. Classifying curved orogens based on timing relationships between structural development and vertical-axis rotations. In: Sussman, A.J., Weil, A.B. (Eds.), Orogenic Curvature: Integrating Paleomagnetic and Structural Analysis: Geological Society of America Special Paper, 383, pp. 1–15.
Wölfler, A., Kurz, W., Fritz, H., Stüwe, K., 2011. Lateral extrusion in the Eastern Alps revisited: refining the model by thermochronological, sedimentary, and seismic data. Tectonics 30, TC4006. https://doi.org/10.1029/2010TC002782.
Yamaji, A., 2003. Are the solutions of stress inversion correct? Visualisation of their reliability and the separation of stresses from heterogeneous fault-slip data. J. Struct. Geol. 25, 241–252.
Yonkee, A., Weil, A.B., 2010. Reconstructing the kinematic evolution of curved mountain belts: internal strain patterns in the Wyoming salient, Sevier thrust belt, U.S.A. GSA Bull. 122 (1/2), 24–49.
Zakariadze, G., Karamata, S., Korokovsky, S., Ariskin, A., Adamia, S., Chkhouta, T., Sergeev, S., Solov'eva, N., 2012. The Early-Middle Palaeozoic Oceanic events along the Southern European margin: the Deli Jovan Ophiolite Massif (NE Serbia) and palaeo-oceanic zones of the Great Caucasus. Turk. J. Earth Sci. 21, 635–668.
Žujović, J., 1886. Geologische Übersicht des Königreiches Serbien. Jahrb. Geol. Bundesanst. 36, 71–126.